JGR Oceans

RESEARCH ARTICLE
10.1029/2021JC017927

Mesoscale and Submesoscale Shelf-Ocean Exchanges Initialize an Advective Marine Heatwave

Ke Chen[1], **Glen Gawarkiewicz**[1], **and Jiayan Yang**[1]

[1]Physical Oceanography Department, Woods Hole Oceanographic Institution, Woods Hole, MA, USA

Key Points:

- Cyclonic eddies in the vicinity of warm-core rings can precondition the outer shelf by changing pressure gradient and inducing frontogenesis
- Upwelling wind can work jointly with cyclonic eddies to drive locally intensified large-magnitude bottom intrusions across-isobath
- Consideration of three dimensionality such as along-shelf bathymetry is essential for a comprehensive understanding of cross-shelf exchange

Correspondence to:

K. Chen,
kchen@whoi.edu

Citation:

Chen, K., Gawarkiewicz, G., & Yang, J. (2022). Mesoscale and submesoscale shelf-ocean exchanges initialize an advective Marine Heatwave. *Journal of Geophysical Research: Oceans*, *127*, e2021JC017927. https://doi.org/10.1029/2021JC017927

Received 25 AUG 2021
Accepted 5 DEC 2021

Author Contributions:

Conceptualization: Ke Chen
Data curation: Ke Chen
Formal analysis: Ke Chen
Funding acquisition: Ke Chen
Investigation: Ke Chen, Glen Gawarkiewicz, Jiayan Yang
Methodology: Ke Chen
Project Administration: Ke Chen
Resources: Ke Chen, Glen Gawarkiewicz
Software: Ke Chen
Validation: Ke Chen
Visualization: Ke Chen
Writing – original draft: Ke Chen
Writing – review & editing: Ke Chen, Glen Gawarkiewicz, Jiayan Yang

Abstract Observations and high-resolution numerical modeling are used to investigate the dynamical processes related to the initiation of an advective Marine Heatwave in the Middle Atlantic Bight of the Northwest Atlantic continental shelf. Both the observations and the model identify two significant cross-shelf intrusions in November 2016 and January 2017, with the latter inducing large-magnitude water mass anomalies across the shelf. Model prognostic fields reveal the importance of the combination of cyclonic eddies or ringlets and upwelling-favorable winds in producing the large-distance cross-shelf penetration and temperature/salinity anomalies. The cyclonic eddies in close proximity to the shelfbreak set up local along-isobath pressure gradients and provide favorable conditions for the intensification of the shelfbreak front, both processes driving cross-isobath intrusions of warm, salty offshore water onto the outer continental shelf. Subsequently, strong and persistent upwelling-favorable winds drive a rapid, bottom intensified cross-shelf penetration in January 2017 composed of the anomalous water mass off the shelfbreak. The along-shelf settings including realistic representation of bathymetric features are essential in the characteristics of the cross-shelf penetration. The results highlight the importance of smaller scale cyclonic eddies and the intricacy of the interplay between multiple processes to drive significant cross-shelf events.

Plain Language Summary This work describes the physical processes initiating a Marine Heatwave (extreme event with large ocean temperature anomalies) on the Northeast US shelf in early 2017. Based on available ocean observations and a new high-resolution (1-km resolution) computer model, we show that the smaller eddies in addition to the commonly known Gulf Stream warm-core rings play an important role in elevating the temperature and salinity at the outer continental shelf. Subsequently, upwelling wind (along-coast wind that moves surface water away from the coast and subsurface water towards the coast) acts upon the elevated temperature and salinity and drives a large-magnitude intrusion across the bottom of the continental shelf near a bathymetric trough. Along-shelf bottom topography effectively shapes the cross-shelf intrusion. This study highlights the intricacy of multiple physical processes in cross-shelf exchange.

1. Introduction

The global climate system has been undergoing profound changes in recent decades. As a key component of the climate system, the coastal ocean has been particularly affected. As the coastal ocean changes are significant in terms of impacts on fisheries, hazards, offshore wind energy, and defense, it is important to understand how the changes that occur on a global scale are manifested in the coastal ocean. In particular, it is imperative to understand the mechanisms connecting the large-scale climate variability with the changes and processes in the coastal oceans.

The coastal ocean in the Northwest North Atlantic (Figure 1) off the Northeast US coast has been in the forefront of some of the most dramatic changes in recent years, including accelerated warming (e.g., Forsyth et al., 2015; Pershing et al., 2015), frequent extreme warm anomalies, also known as Marine Heatwaves (e.g., Chen, Gawarkiewicz, et al., 2014; Chen et al., 2015, 2016), and faster sea level rise (e.g., Piecuch et al., 2018; Sallenger et al., 2012). Further offshore, the Gulf Stream destabilization point, where the Gulf Stream starts to develop larger magnitude meanders, is shifting westward (Andres, 2016), which implies that this major western boundary current has a larger chance of directly impacting the outer continental shelf (e.g., Gawarkiewicz et al., 2012). Meanwhile, increased number of Gulf Stream warm core rings (Gangopadhyay et al., 2019), as well as intense salinification (Holliday et al., 2020) have also been reported off the shelfbreak of the Northwest Atlantic. These dramatic changes potentially have significant impacts on the large marine ecosystem (LME) in the region, which supports some of the most commercially valuable fisheries in the world. Already, shifting fish populations and

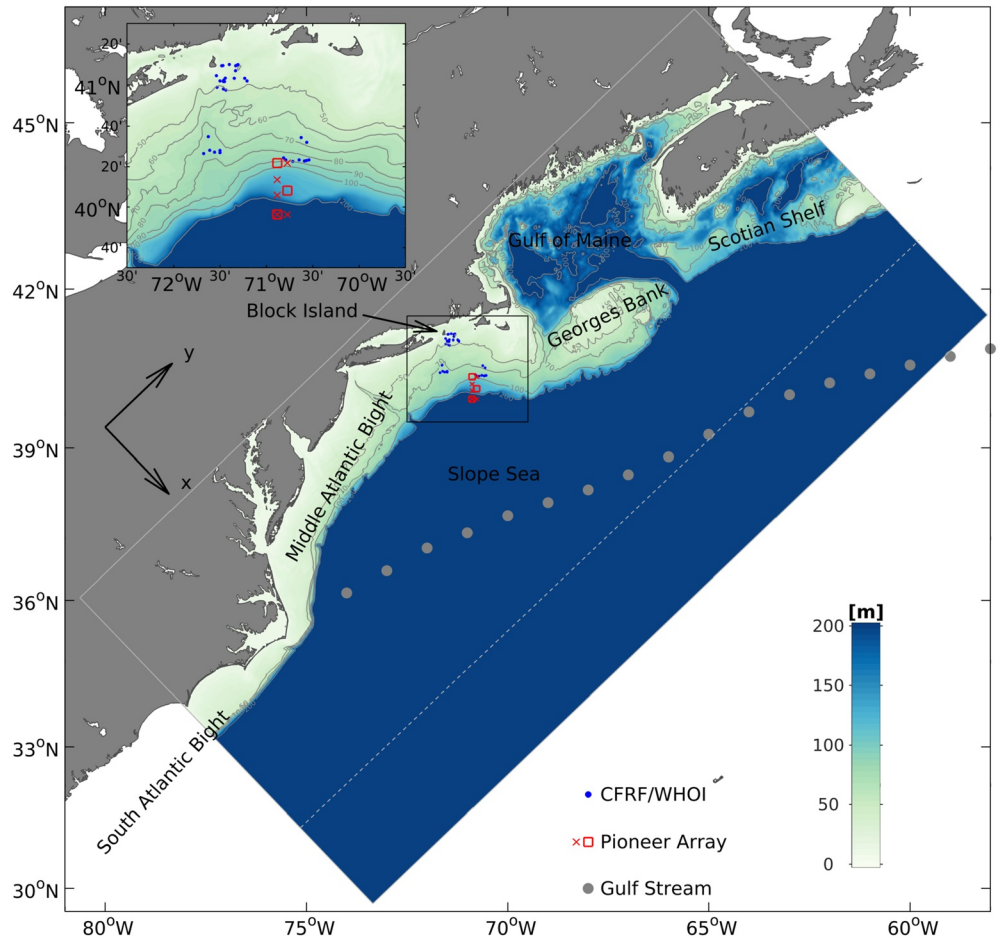

Figure 1. Map showing the domain of study. Model bathymetry is shown in color with 50-, 70-, 100-, and 200-m isobaths contoured in gray. A blow-up of the southern New England shelf shows more detailed bathymetry with 50-, 60-, 70-, 80-, 90-, 100-, and 200-m isobaths contoured. The model domain is bounded by the solid gray lines. The dashed gray line represents the open boundary of the previous MABGOM/MABGOM2 model (Chen & He, 2015). Locations of temperature and salinity profiles from the CFRF/WHOI Shelf Fleet data collection (see Section 2.1) are shown in blue. Ocean Observatories Initiative (OOI) Pioneer Array mooring sites are marked in red with square representing surface mooring and cross representing profiler mooring. The long-term mean Gulf Stream path (defined as the location of 15°C isotherm at 200 m [e.g., Joyce et al., 2009]) is denoted by the gray dots. Major geographic locations are labeled. A local Cartesian coordinate system for cross-shelf and along-shelf momentum balance (Section 3.2) is also defined.

geographic distributions have been reported (e.g., Lucey & Nye, 2010; Nye et al., 2009), presumably related to both long-term trends as well as extreme events. Therefore, a better understanding of how these different recent changes are connected is of both scientific interest and societal importance.

Extreme and positive temperature anomalies, sometimes referred to as Marine Heatwaves, can have a profound impact on the ocean environment around the world (e.g., Benthuysen et al., 2020), and have been occurring frequently in the NW Atlantic coastal ocean (Chen et al., 2014a, 2015; Gawarkiewicz et al., 2019; Mills et al., 2013; Pershing et al., 2018; Schlegel et al., 2021). In early 2017, CTD (conductivity, temperature, and depth) observations collected by commercial fishing vessels as part of a community science program (Gawarkiewicz & Mercer, 2019), revealed an advective Marine Heatwave on the southern New England shelf in the Middle Atlantic Bight (MAB). During this advective heatwave, depth-averaged temperature anomalies were more than 4°C above the 90th percentile of historical values in the region (Gawarkiewicz et al., 2019). The depth-averaged salinity anomaly was also above the 90th percentile by ~1, indicating that this was a compound event with large anomalies in both temperature and salinity. The anomalous water mass was advected by the equatorward mean along-shelf flow, persisted through the along-shelf advective pathway in the MAB, and flowed off the shelf near Cape Hatteras in April 2017, lasting for ~4 months over the continental shelf. The large salinity anomaly in addition

to the temperature anomaly strongly suggests an origin in the Gulf Stream associated with the intrusion of warm, salty water. Indeed, satellite sea surface temperature (SST) images show that multiple Gulf Stream warm-core rings (WCRs) detached from the Gulf Stream and came in close proximity to the outer continental shelf from November 2016 to February 2017 (cf. Figure 5 in Gawarkiewicz et al., 2019). Because WCRs have been shown to be one major forcing mechanism for shelfbreak exchange (e.g., Chen, He, et al., 2014; Garfield & Evans, 1987; Joyce et al., 1992; Zhang & Gawarkiewicz, 2015, among many others), it was hypothesized that Gulf Stream WCRs are the driver of the anomalous intrusion and associated water mass anomalies from the outer shelf to the inner shelf off southern New England (Gawarkiewicz et al., 2019). While this is certainly a reasonable hypothesis, a thorough proof using existing data is not possible due to the limitation of available observations. In particular, important questions remain to be answered: whether or not WCRs are indeed important for the water mass anomalies on the shelf, what the exact working of the physical processes underlying the cross-shelf penetration of the anomaly is, and what roles other factors, for example, atmospheric forcing, have played during this event. Highly anomalous water mass properties over the inner shelf of southern New England was also noted previously based on an analysis of mooring data and shipboard hydrography in November 2009 (Ullman et al., 2014). They noted that no previous observations contained near bottom salinities as high as that observed in November 2009. Similarly, impingement of a Gulf Stream warm-core ring at the shelfbreak was considered to be responsible, although the exact cause of this event is not entirely clear (Ullman et al., 2014). Detailed investigations of such extreme events in the coastal ocean will improve our understanding of how the coastal ocean changes are connected to local and offshore forcings and how these processes might be changing in the context of regional and global changes described above.

In this study, we combine observations and a new high-resolution regional model to unravel the dynamical processes for the initiation of the observed water mass anomalies over the continental shelf. We first examine the existing observations during November 2016 and February 2017 to further evaluate the spatiotemporal characteristics of the anomalies, and compare the observations with the climatological mean conditions. Next, we describe the setup of the newly developed regional model and demonstrate the model's capacity in resolving the unusual intrusions and anomalies. We then use the model prognostics and diagnostics to understand the dynamics of relevant processes causing the anomalies. The goal of this case study is to provide improved understandings of shelf-ocean exchange, to motivate future studies looking into interannual and longer-term variability of extreme events in the context of climate change, and to offer potential insights into processes in other similar coastal settings.

2. Observations and Modeling

2.1. Observational Data

2.1.1. The CFRF/WHOI Shelf Research Fleet Hydrographic Data

The temperature and salinity profiles are collected as part of a community science program, the Shelf Research Fleet (Gawarkiewicz & Mercer, 2019), a collaboration between the Woods Hole Oceanographic Institution (WHOI) and the Commercial Fisheries Research Foundation (CFRF). This observational effort measures vertical profiles of temperature and salinity over the continental shelf at bi-weekly intervals. Sampling is conducted by commercial fishers using a suite of RBR Instruments Concerto Conductivity-Temperature-Depth (CTD) sensors. The data from this project are used to better understand both year-to-year variability of ocean thermohaline structure as well as the changing nature of seasonal transitions and extrema over the continental shelf south of New England. The data have been collected since November 2014 and have been quality controlled at WHOI (F. Bahr) with sensors regularly calibrated at the RBR facilities in Ontario, Canada. A total of 36 profiles collected between November 2016 and February 2017 were used in this study. The locations of the profiles can be found in Figure 1.

2.1.2. Northwest Atlantic Regional Climatology

The National Centers for Environmental Information (NCEI) Northwest Atlantic (NWA) regional climatology is a product derived from the World Ocean Database (WOD) providing high-resolution, quality-controlled multidecadal climatological conditions for the Northwest Atlantic (Seidov et al., 2016). The data set is comprised of objectively analyzed temperature and salinity fields at standard levels. The data used in this work are monthly temperature and salinity climatologies based on historical profiles from 1955 to 2012 at 1/10° resolution.

2.1.3. Pioneer Array

The Ocean Observatories Initiative (OOI) Pioneer Array (Figure 1) south of New England has been in continuous operation since January 2016. The array consists of seven mooring sites between the 90 and 440 m isobaths along with a number of gliders deployed at the Eastern Boundary (EB), the Frontal Zone (FZ), and over the slope region to resolve rings and eddies over the continental slope. There are four moorings in a north-south line and three moorings 9 km to the east providing information on along-shelf gradients. The mooring sites were chosen to minimize disruption to the intense fishing activity in the region by locating two mooring sites over known shipwrecks after consultation with the commercial fishing industry. The seven mooring sites contain both profilers with CTDs and Nortek current meters as well as bottom-mounted ADCPs (Acoustic Doppler Current Profiler). Lockheed RDI Workhorse Sentinel 150 kHz ADCPs are deployed at the Onshore and Central Surface Mooring Sites at the Multi-Function Nodes on the bottom and a Workhorse Long Ranger Sentinel 75 kHz ADCP is deployed at the Offshore Surface Mooring at the Multi-Function Node near the bottom. Three of the sites are also equipped with surface moorings that telemeter data in real time via satellites and also contain meteorological sensors that measure wind speed and direction as well as radiometers and humidity sensors to allow the calculation of air-sea heat fluxes (e.g., Chen et al., 2018). Mooring turn-around cruises provide additional hydrographic sampling. The scientific rationale and conceptual design of the Array are documented by Gawarkiewicz and Plueddemann (2020), as well as technical details regarding the instrumentation and sensors. Further information on the instrumentation and sensors may be found at oceanobservatories.org/array/coastal-pioneer-array.

2.2. Numerical Modeling

2.2.1. New Regional Model Development and Configuration

A new high-resolution regional circulation model encompassing the shelf and slope regions off the Northeast U.S., that is, NESS model, was constructed based on the hydrostatic Regional Ocean Modeling System (ROMS), which is a free-surface, primitive equation model in widespread use for estuarine, coastal, and basin-scale ocean applications (www.myroms.org/papers). The purpose of developing this new NESS model is to capture meso- to submeso-scale processes better in the Northwest North Atlantic shelf-slope region, particularly those associated with cross-shelf exchange processes. The development of this new high-resolution model is based on prior modeling experience of MABGOM and MABGOM2 models, which have been successfully used to investigate shelf and slope processes in the region (Chen et al., 2015, 2016; Chen & He, 2015; Rypina et al., 2019). The horizontal resolution of the new NESS model is *1-km* in both cross-shelf and along-shelf directions. Vertically, there are 40 terrain-following layers with a stretching scheme to resolve both surface and bottom layers (minimum resolution less than 1 m) and the water column. Sensitivity experiments are carried out in choosing relevant numerical parameters (e.g., baroclinic and barotropic time steps, background diffusivity) to accommodate the higher-resolution configuration. A generic-length scale (GLS) turbulent mixing closure k-kl scheme (Warner et al., 2005) is used to calculate vertical mixing. Bottom stress is calculated using a quadratic term with a drag coefficient of 0.003. The main advantages of the new NESS model compared to the previous MABGOM2 model are the aforementioned higher horizontal resolution and a more offshore location of the southeast open boundary (Figure 1), allowing better representations of the Slope Current (Flagg et al., 2006), Gulf Stream, and their interactions.

The configuration of the initial and open boundary conditions as well as surface forcing follows the same strategy of prior modeling work (e.g., Chen et al., 2015; Chen & He, 2015). The model initial conditions are extracted from a product that combines the mesoscale variability from a data assimilative global ocean circulation model, Hybrid Coordinate Ocean Model (Chassignet et al., 2006) plus Navy Coupled Ocean Data Assimilation (HYCOM/NCODA, GOFS3.0), with the background mean fields from the temperature and salinity climatology of the World Ocean Atlas (WOA) climatology. The rationale of this procedure is to remove the mean temperature and salinity biases in the global product, which is not optimized for shelf- and/or slope-scale dynamics due to under-represented coastal processes including river freshwater flux and tides. In the correction, the climatological monthly means of temperature and salinity from the HYCOM/NCODA data set were replaced by climatological monthly means from the WOA climatology while the variability, that is, the deviations from the climatological mean, was retained. In addition, temperature and salinity from the open ocean (deeper than 2,000 m) in the NESS model were nudged back to the corrected, four-dimensional temperature/salinity field from HYCOM/NCODA. The nudging time scale is 2 days at the open boundary and increases linearly to a much longer time scale approaching infinity at the 2,000 m isobath, which results in nudging strength decreasing gradually from

the open boundary toward the interior. No nudging was applied in regions of water depth shallower than 2,000 m. Generally, the data assimilative HYCOM/NCODA provides good estimates of the mesoscale variability in the open ocean, particularly for the Gulf Stream meanders and WCR in the slope sea. With the temperature and salinity nudging in the Gulf Stream/Slope Sea region, the model is able to capture realistically the meandering of the Gulf Stream and the hydrography in the open ocean and is able to provide important offshore conditions for shelf processes. The 2,000 m isobath generally follows the orientation of the shelf break (~200 m isobath), and the distance between the shelf break and 2,000 m isobath varies from 50 to 70 km, larger than the characteristic spatial scales (10–30 km) in this region (Todd et al., 2012). Therefore, the nudging only constrains conditions in the open ocean and allows dynamical processes to evolve freely exchanging water masses between the open ocean and the shelf.

Subtidal free surface and 2D momentum boundary conditions of the NESS model were derived from the corrected HYCOM/NCODA fields using an explicit Chapman (1985) and Shchepetkin scheme (Mason et al., 2010), plus M2 tidal harmonics from the TPXO9 version 4 global tidal model (Egbert & Erofeeva, 2002). An Orlanski-type radiation (Orlanski, 1976) boundary condition was used for 3D state variables.

The surface forcing of the model combines air-sea flux calculated using bulk formulae and a surface thermal correction based on high-resolution SST maps. This scheme has been applied previously to provide realistic forcing of air-sea exchange (Chen et al., 2015; Chen & He, 2010). The bulk formulae calculation (Fairall et al., 2003) is based on three hourly and 0.125° resolution meteorological data (surface winds, air temperature, air pressure, relative humidity, short wave radiation, long wave radiation, cloud coverage, and precipitation) from the European Centre for Medium-Range Weather Forecasts (ECMWF) ERA5 global reanalysis (Hersbach et al., 2020). This calculation provides large-scale variability in the fluxes of momentum and buoyancy at the ocean surface, but may contain uncertainties in reproducing some fine scale structures. To compensate for this deficiency in the surface forcing, the surface thermal correction adjusts the surface heat flux based on the difference of the model SST and the 1 km resolution multi-scale ultra-high resolution (MUR) SST (Chin et al., 2017). The adjustment time scale is 3 hours (Chen et al., 2015), consistent with the temporal resolution of the ERA5 product.

Fresh water runoff from nine major rivers in the region was also imposed. These include the St. John, Penobscot, Kennebec, Androscoggin, Merrimack, Connecticut, Hudson, Delaware, and Potomac Rivers. For each river, United State Geological Survey (USGS) real-time runoff measurements were used to specify freshwater volume transport and temperature.

2.2.2. Model-Data Comparison

Although the main purpose of the realistic modeling is to develop a better understanding of the dynamical processes, and to a lesser extent, to reproduce the observations exactly, it is informative to assess the model skill in resolving the relevant processes. Because of the prior successful constructions and applications of the MABGOM and MABGOM2 models, based on which the NESS model is built, and because of the increased resolution, it is reasonable to expect that the new NESS model has improved capability to capture multi-scale processes in the NW Atlantic shelf-slope region. For the demonstration of the model skill, 4-dimensional temperature and salinity are compared against the Shelf Research Fleet profiles, that is, the model and observations are compared at exactly the same time and location. The modeled temperature and salinity fields compare very well with the observations (Figure 2). The seasonal cooling of the shelf water is accurately captured, and in particular, the model reproduces the bottom intensified intrusions of warm and salty slope water (Section 3.1) in November 2016 and January 2017. Both the magnitudes and depth-structures agree reasonably well. Overall root mean square error (RMSE) of temperature (salinity) is 0.8 (0.4), confirming the improved skill of the new NESS model.

3. Dynamics of the Cross-Shelf Intrusions

3.1. Characteristics of the Temperature and Salinity Anomalies

From November 2016 to February 2017, 36 temperature and salinity profiles were collected on the southern New England shelf (Figure 1), which provide valuable information about the water mass anomalies in the region. For comparisons, the profiles are clustered into two groups: inner shelf profiles located shoreward of the 50 m isobath, and mid/outer shelf profiles located seaward of the 50 m isobath. Each profile is compared against the corresponding climatological condition in the NWA regional climatology. Although the profiles are not evenly

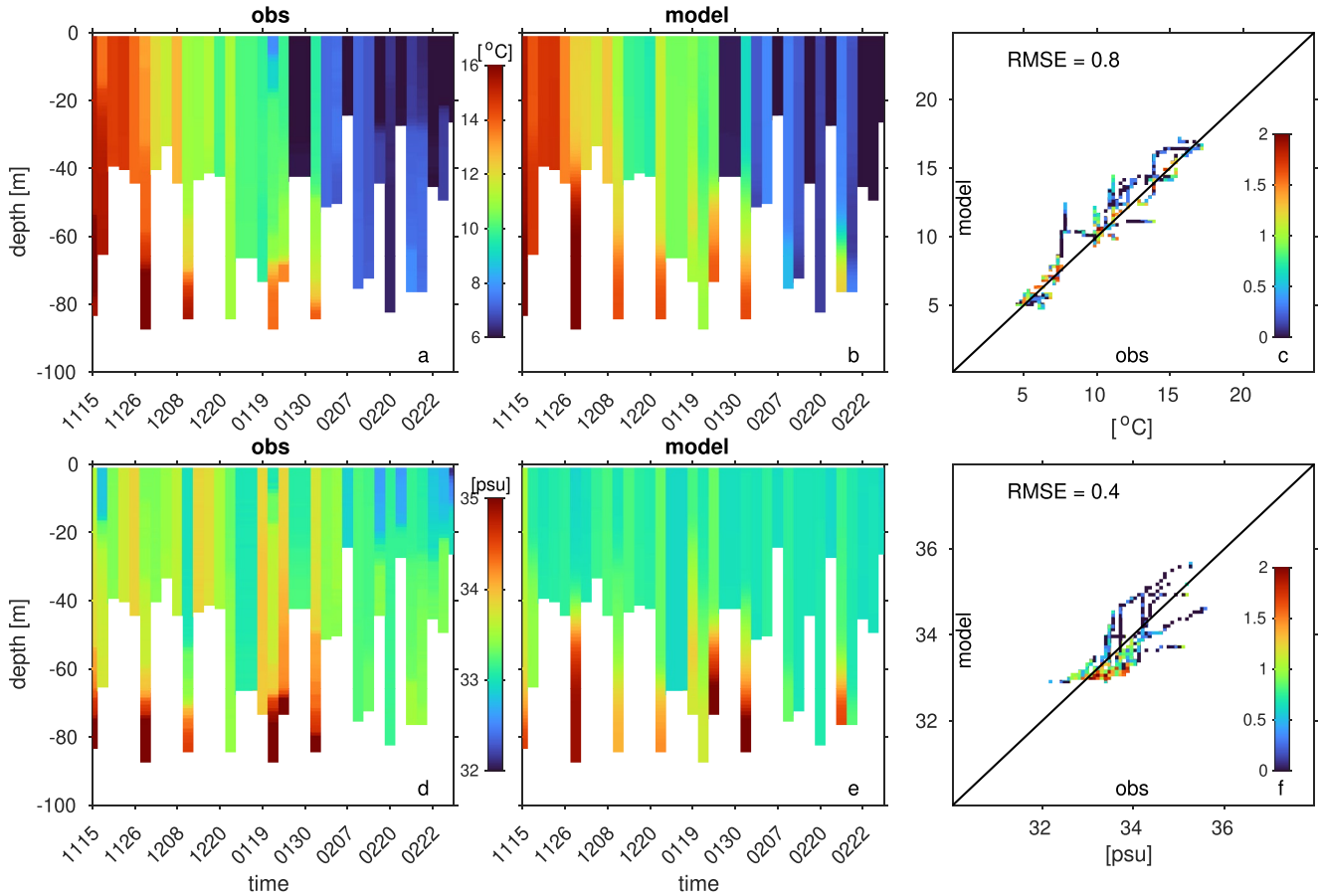

Figure 2. Comparison of temperature and salinity between CFRF/WHOI profiles (a), (d) and the model (b), (e) from November 2016 to February 2017. One-on-one plots (c), (f) with root mean square error (RMSE) show the overall comparisons. Colorbars in panel c and f are in the logarithmic scale for the number of points in each 0.25°C × 0.25°C box for temperature and 0.08 × 0.08 for salinity. Note the time axis is not linear.

distributed in time, it appears that at least two periods of anomalous conditions are captured by the observations at the middle and outer shelf–one in November 2016 and the other one in January 2017 (Figure 3). The maximal anomaly of temperature is larger than 5.6°C, and maximal salinity anomaly is larger than 1.7. The anomalies are bottom intensified, but also extend through the water column, suggesting that the anomalies are ultimately associated with the intrusions of offshore warm salty waters. This is verified by the salinity profiles recorded by the wire-following profiling moorings from the Pioneer Array (Figure 4). At the central inshore site (~127 m isobath, Figure 1), high salinity signals were recorded in November 2016 and January 2017 as two distinct events, with higher salinity toward the bottom exceeding 34.5, which is a typical value for the shelfbreak front (e.g., Linder & Gawarkiewicz, 1998). This implies that the foot of the shelfbreak front or the subsurface slope water moved further onshore. Indeed, salinity recorded at the upstream inshore site at the ~95 m isobath also reveals high salinity waters in November 2016 and January 2017, despite weaker intensity and smaller vertical scales (Figure 4). The consistent timing of high salinity signals at the central inshore site and upstream inshore site, along with the depth structure of the CTD profiles at the middle/outer shelf (Figure 3) suggests that anomalous water masses resulted from cross-shelf exchange processes that occurred during November 2016 and January 2017, which originated at the shelfbreak but penetrated large distances onshore.

CTD profiles collected at the inner shelf provide additional information about the spatiotemporal characteristics of the water mass anomalies (Figure 5). In comparison to the middle/outer shelf profiles, the temperature and salinity during November 2016 to February 2017 were both above the long-term climatology. While high temperature can be expected in the context of long-term warming of the Northwest Atlantic coastal ocean (Chen et al., 2020), the large salinity anomalies at such shallow locations would almost certainly be caused by the intrusion of offshore waters as freshwater flux at the air-sea interface, that is, evaporation-minus-precipitation,

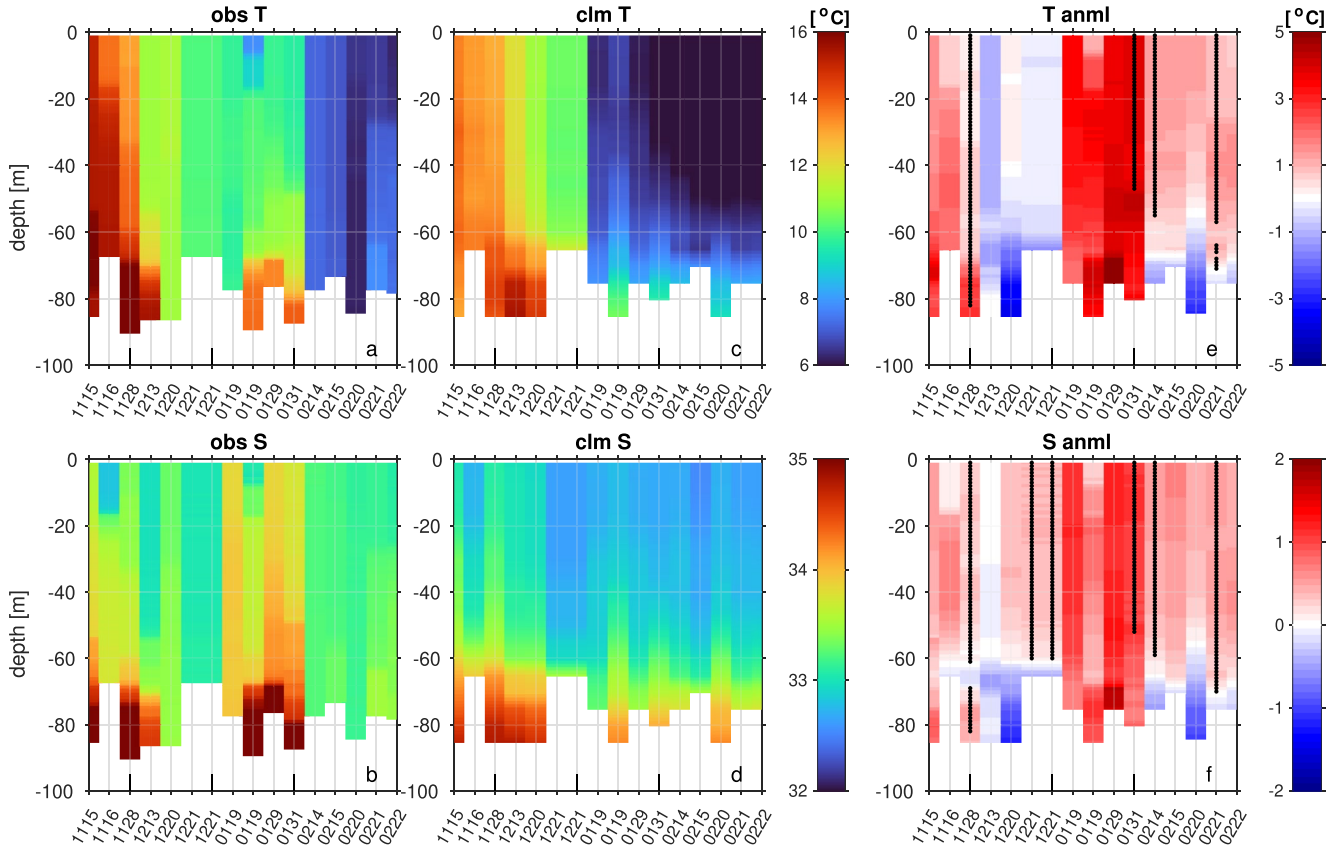

Figure 3. Temperature and salinity profiles (a and b) compared with climatological conditions (c and d) at the outer and middle shelf. The anomaly (observation minus climatology) are shown in panel (e) and (f) Anomalies larger than 2 standard deviations are marked in black. The short vertical bars on the *x*-axis denote the different months. Note the time axis is not linear.

is negligible in the regional salt budget (Lentz, 2010). Although only two profiles were collected in November 2016 and only one profile was collected in January 2017 at this inner shelf location, the salinity anomaly is clearly visible from these three profiles (Figure 5). It is also worth noting that salinity at all depths in December 2016 is clearly larger than the long-term mean values, suggesting either offshore intrusions in November 2016 at the southern New England shelfbreak or upstream (poleward) may have reached this nearshore region.

Gulf Stream WCRs have long been identified as a significant player in the shelf-ocean exchanges (e.g., Chen, He, et al., 2014; Cherian & Brink, 2016; Garfield & Evans, 1987; Joyce et al., 1992; Lee & Brink, 2010; Morgan & Bishop, 1977; Zhang & Gawarkiewicz, 2015). Limited satellite SST images do show multiple WCRs during November 2016 to February 2017 (Gawarkiewicz et al., 2019), suggesting that these anticyclonic eddies may be important for the presence of the anomalous water mass on the shelf during this period. In the following, we investigate in detail the processes by which offshore warm and salty waters penetrate onto the shelf and show that multiple processes instead of WCRs alone can work collectively in a synchronized manner to drive the significant onshore intrusion of the anomalous warm and salty water mass.

3.2. Intrusion at the Outer Shelf Associated With Cyclonic Eddies

Two periods with significant shelfbreak exchange are reproduced by the NESS model: one in mid to late November, and the other one during mid to late January, consistent with the observations (Section 3.1). As will be discussed below, the intrusions crossing the shelfbreak during these two periods are both associated with cyclonic circulation patterns adjacent to the shelfbreak.

During November 2016, a WCR was located in the slope sea off the southern New England shelf, translating southwestward before being absorbed by the Gulf Stream in early December. The NESS model reproduces this

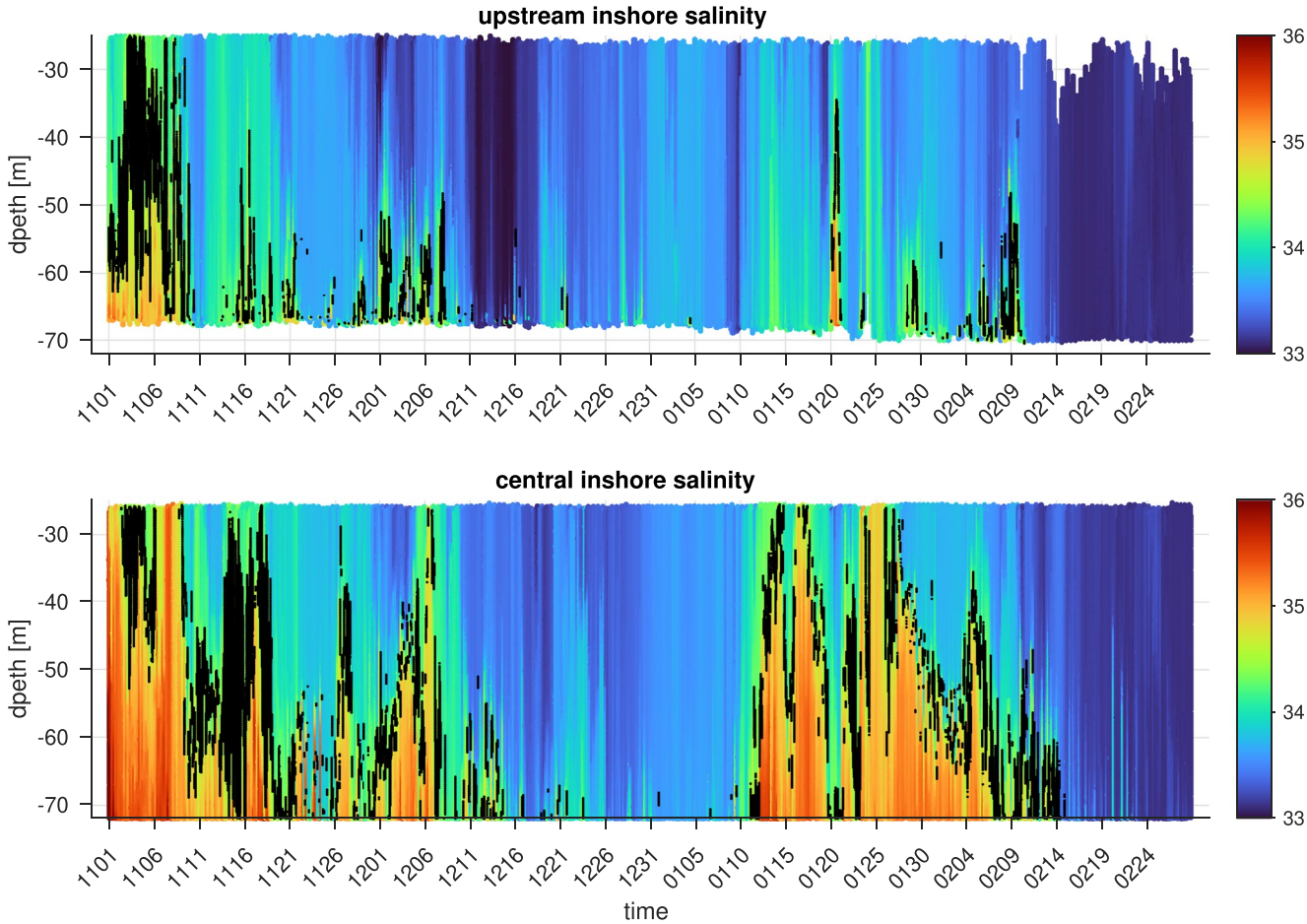

Figure 4. Salinity recorded by the wire-following profiler at the upstream inshore (~95 m isobath, top panel) and central inshore (~127 m isobath, bottom panel) sites of the Pioneer Array during November 2016 to February 2017. The 34.5 isohaline is marked in black to highlight the boundary between the shelf and slope waters.

evolution, and the spatiotemporal patterns of modeled SST and free surface compare well with the satellite derived SST (e.g., Figure 6 vs. Figure 7a) and gridded absolute dynamic topography at spatial scales resolved by the altimetry product from Copernicus Marine Environment Monitoring Service (not shown). However, what the satellite observations do not clearly show but the NESS model reveals are the cyclonic eddies surrounding the WCRs (Figure 7). On November 13, 2016, a WCR was centered to the south of Georges Bank and was not directly impinging upon the shelfbreak, although the warm and salty water extended beyond the core. In contrast, two cyclonic eddies to the northwest of the WCR were in direct contact with the shelfbreak (Figure 7b). Comparing with satellite SST, the cyclonic circulation can also be gleaned from the lower surface temperature around 69.5°W and also 71.5°W (Figure 6a). On January 15, 2017, another WCR was in close proximity to the southern New England shelfbreak around 70°W (Figure 6b). A band of cooler water was surrounded by the WCR to the south and a band of warm water to the north toward the shelfbreak, indicating a cyclonic circulation pattern acting between the WCR and the shelfbreak. The NESS model also confirms this cyclonic pattern (not shown), which lasted ~ 20 days before being displaced by the WCR.

These cyclonic eddies likely formed from the interactions of the mesoscale flows including the WCRs with ambient currents and have smaller horizontal scales (~10–50 km in diameter) than the WCRs. The timescale of these cyclonic eddies is generally shorter than that of WCRs, but they persist for ~10–20 days before losing coherence and dissipating into the background currents. Because of the smaller spatial and temporal scales, cyclonic eddies in the vicinity of Gulf Stream WCRs are difficult to identify in observations. Current satellite altimetry measurements generally do not have sufficient resolution to capture these smaller mesoscale features and SST imagery alone is not always able to reveal the existence of these cyclones as they do not necessarily have identifiable surface thermal signature and even if they do SST alone does not necessarily reveal surface flow

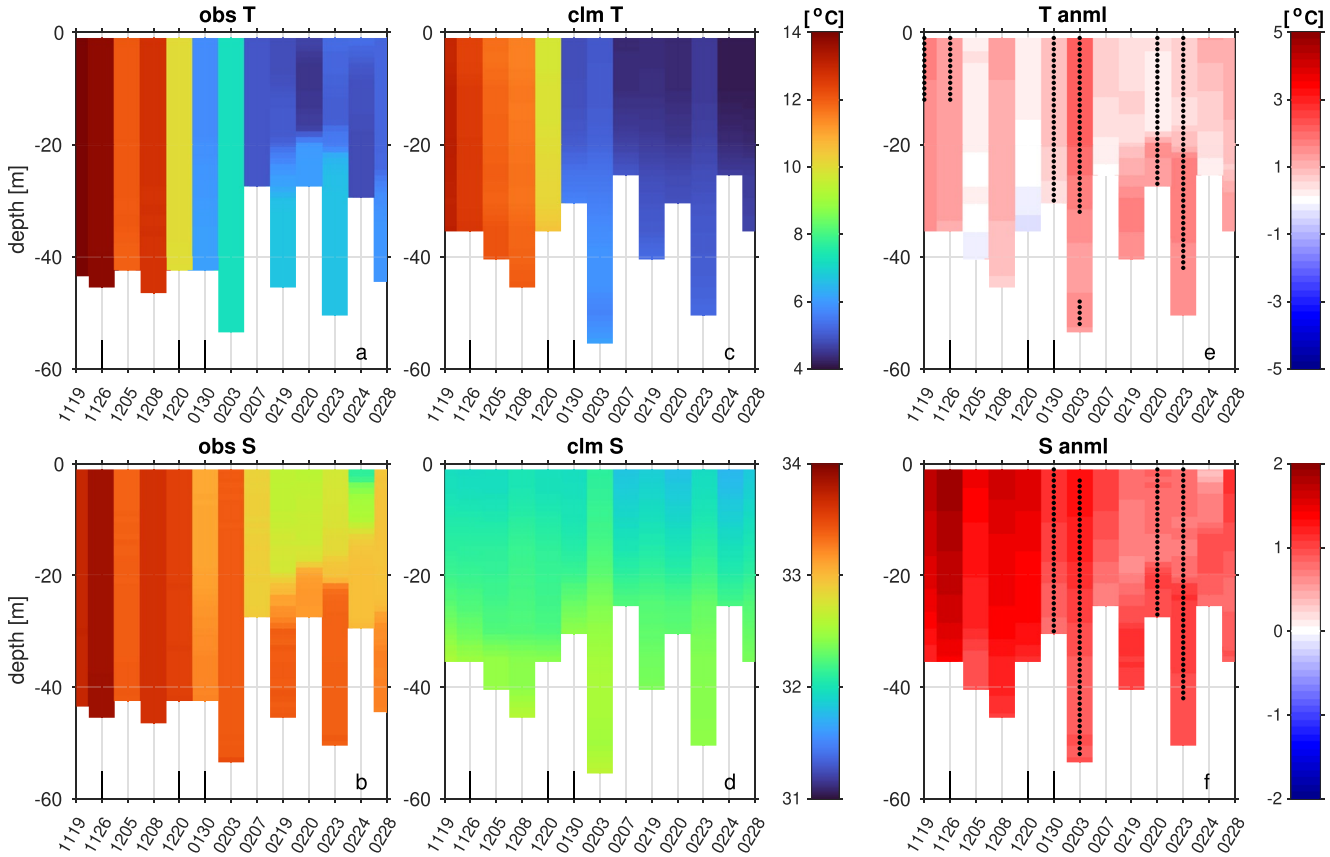

Figure 5. Temperature and salinity profiles (a and b) compared with climatological conditions (c and d) at the inner shelf. The anomaly (observation minus climatology) is shown in panels (e) and (f) Anomalies larger than 2 standard deviations are marked in black. The short vertical bars on the *x*-axis denote the different months. Note the time axis is not linear.

patterns. Nevertheless, in situ field measurements during the Warm Core Ring Program in the 1980s do reveal cyclonic eddies in addition to the anticyclonic WCRs (Churchill et al., 1986; Joyce, 1984; Kennelly et al., 1985), which are more prominent features between the Gulf Stream and the continental shelf and thus could overshadow the cyclonic eddies. Both Joyce (1984) and Kennelly et al. (1985) report smaller cyclonic eddies outside in the northeast quadrant of the WCRs 81D and 82B, translating anti-cyclonically around the periphery of the WCRs. On the other hand, Churchill et al. (1986) report a cyclonic eddy to the west of WCR 83D and attribute the formation of the cyclonic eddy to processes associated with anticyclone-cyclone vortex pairs, that is, modons (Flierl

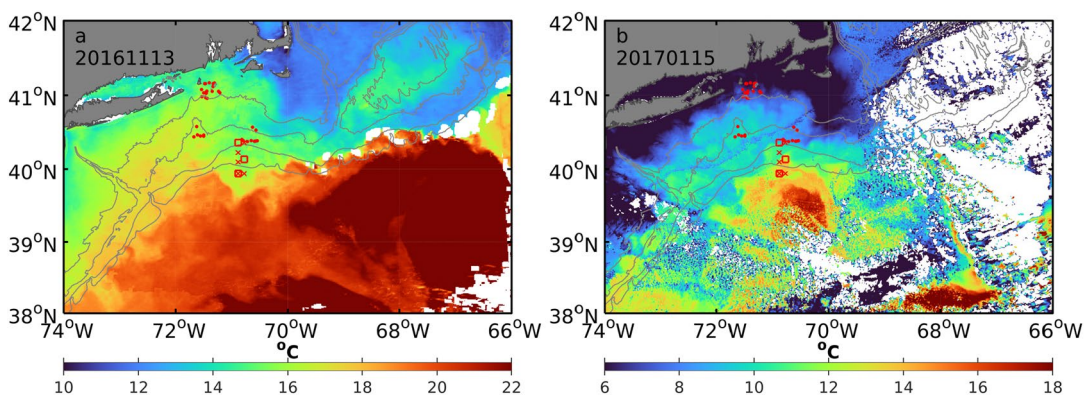

Figure 6. Daily composite sea surface temperature from AVHRR on November 13, 2016 and January 15, 2017. 50, 70, 100, and 200 m isobaths are contoured in gray.

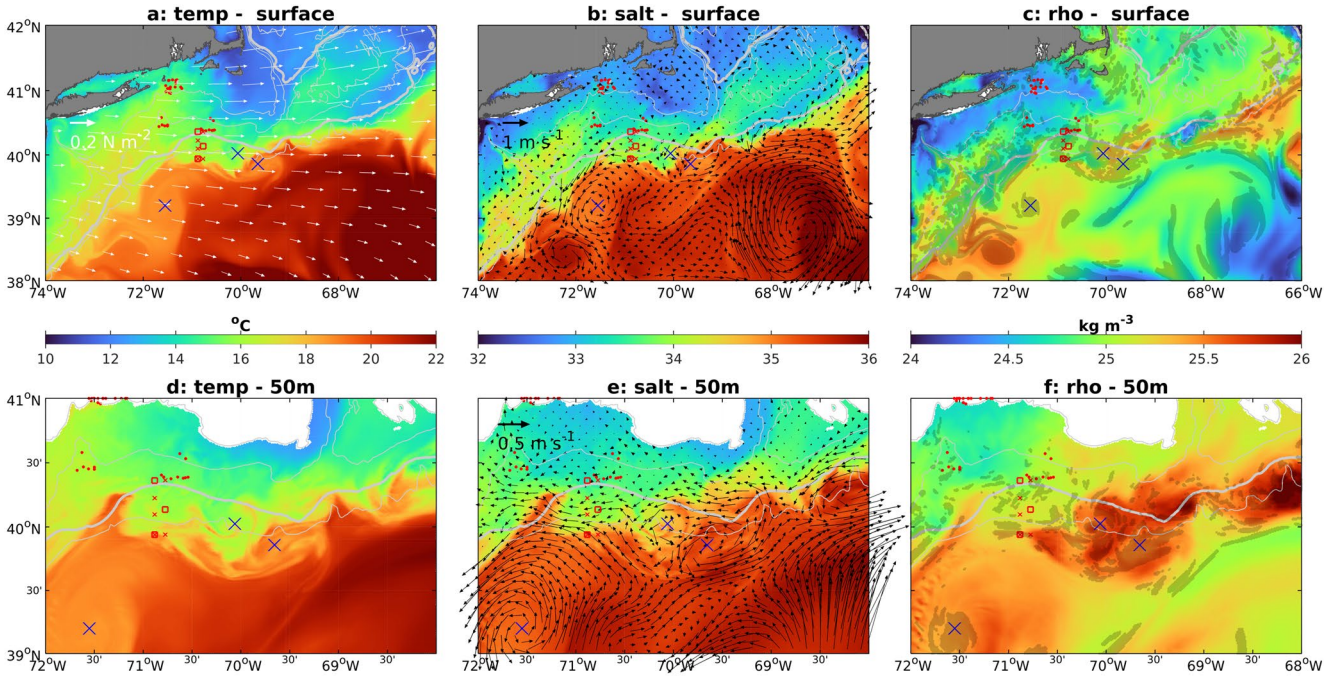

Figure 7. Model temperature (a), (d), salinity with subtidal currents (b), (e) and density with locations of relative vorticity larger than 0.3 *f* marked in shade (c), (f) on November 13, 2016. Panels (a–c): plane view at surface. Panels (d–f): plane view at 50 m. Wind stress vectors in white are overlaid in panel (a). All vectors are subsampled to aid visualization. 50, 70, 100, and 200 m isobaths are contoured in gray with 100 m isobath in thicker contour. Locations of CFRF/WHOI profiles and Pioneer Array mooring locations are also marked in red in each panel. Blue crosses denote the locations of cyclonic eddies.

et al., 1983). The cyclonic eddies resolved in the NESS model are certainly comparable to those reported in these earlier studies.

3.2.1. Pressure Gradient Changes

Despite smaller spatial and temporal scales, the cyclonic eddies resolved by the NESS model play an important role in the exchanges across the shelfbreak. The mean flow on the shelf and upper slope is along-isobath, equatorward and largely geostrophic (e.g., Lentz, 2008a). Because adiabatic geostrophic flows cannot cross isobaths, that is, Taylor-Proudman theorem (Brink, 2016), significant shelfbreak exchanges are normally rare and must be associated with ageostrophic processes like external forcing and nonlinear advection. With relative vorticity larger than 0.3*f* (Figures 7c and 7f, peak value above 0.6*f*), the two cyclonic eddies along the shelfbreak at 71.5°W and 69.5°W during November 2016 certainly have the capability to facilitate cross-isobath flow. While the onshore intrusion of offshore water is less apparent at the surface, intrusion of warm, salty waters can be easily identified in the subsurface layer at 50 m (Figures 7d and 7e). In particular, two locations of enhanced intrusions are associated with the presence of the two cyclonic eddies along the shelfbreak. At the leading (northeast) edge of the cyclone at ~69°W, a band of offshore water crosses the shelfbreak and penetrates to ~70 m isobath, accompanied by the cross-isobath flow at 50 m depth. This cross-shelf intrusion appears to be associated with the interaction of the mesoscale flows including the cyclonic eddy at ~69.5°W, the WCR centered around 67°W and another cyclonic circulation pattern at ~68°W close to the 200 m isobath (Figure 7e). Another band of warm, salty water penetrating across the 100 m isobath from the slope sea is located between 71.5°W and 71°W, also at the leading edge of a cyclone. Cross-shelf velocity also reveals a third site of onshore intrusion slightly to the east of 70°W, with weaker cross-shelf extent and smaller temperature/salinity contrasts. The intrusion at this location is nevertheless associated with a cyclonic eddy, although its magnitude is much less. The width of these warm and salty filamentary intrusions range from 10 to 30 km, and is comparable to the spatial scale of intrusions observed at the southern flank of Georges Bank (Lee & Brink, 2010), which is ~20 km. What is different, however, is that the observed filament at Georges Bank is not associated with any identifiable cyclonic eddies, and the intrusion there appears to be surface trapped whereas the intrusions discussed here either have a barotropic character or occupy the majority of the sub-surface water column. Because of the ageostrophic nature of the observed Georges

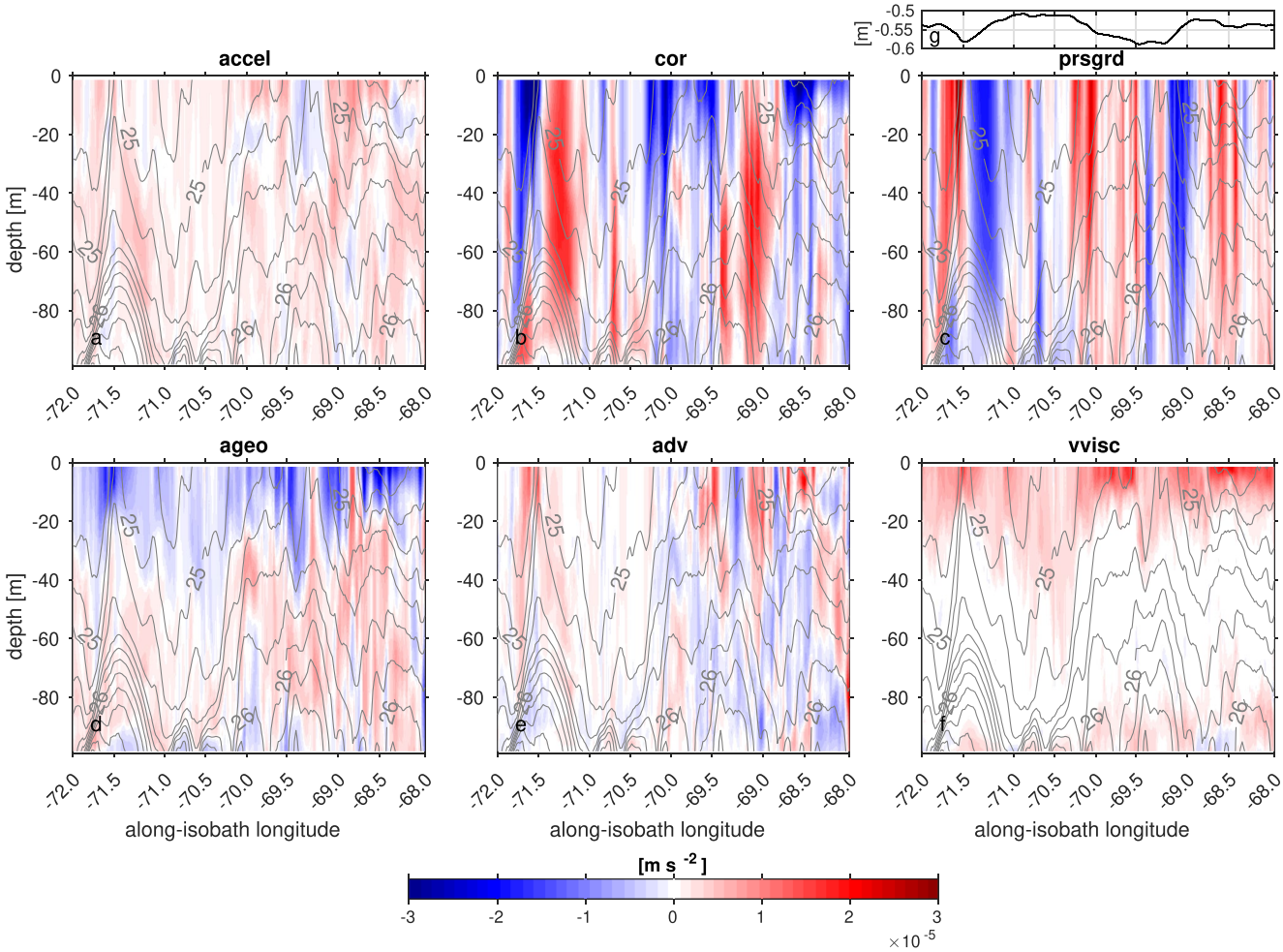

Figure 8. Along-isobath momentum balance at 100 m isobath on November 13, 2016: (a) acceleration (*accel*), (b) Coriolis (*cor*), (c) pressure gradient (*prsgrd*), (d) ageostrophic (*ageo*), (e) advection (*adv*), and (f) vertical viscosity (*vvisc*) terms. Density field is contoured in gray with contour interval 0.2 kg m^{-3}. Along-isobath sea surface height is plotted in panel (g). Negative pressure gradient means higher pressure poleward. Positive Coriolis term means onshore flow.

Bank filament (Rossby number 0.2–0.3), and its similarity to Gulf Stream filaments ("shingles") in the South Atlantic Bight (e.g., Bane et al., 1981; Glenn & Ebbesmeyer, 1994; Lee et al., 1981), mixed barotropic-baroclinic instability was considered as the process underlying the filaments observed at Georges Bank (Lee & Brink, 2010; Luther & Bane, 1985).

Diagnosis of the momentum balance further reveals the dynamics of these cross-isobath flows. In a local cartesian coordinate system (see Figure 1), the cross-shelf and along-shelf momentum balances at the 100 m isobath are:

$$\frac{\partial u}{\partial t} = fv - \frac{1}{\rho_o}\frac{\partial p}{\partial x} - \mathbf{u}\cdot\nabla u - w\frac{\partial u}{\partial z} - A_H\left(\frac{\partial^2}{\partial x^2} + \frac{\partial^2}{\partial y^2}\right)u + \frac{\partial}{\partial z}\left(K_v\frac{\partial u}{\partial z}\right) \quad (1)$$

$$\frac{\partial v}{\partial t} = -fu - \frac{1}{\rho_o}\frac{\partial p}{\partial y} - \mathbf{u}\cdot\nabla v - w\frac{\partial v}{\partial z} - A_H\left(\frac{\partial^2}{\partial x^2} + \frac{\partial^2}{\partial y^2}\right)v + \frac{\partial}{\partial z}\left(K_v\frac{\partial v}{\partial z}\right) \quad (2)$$

Where u and v are defined as cross-isobath (positive offshore) and along-isobath (positive poleward), f is the Coriolis parameter, ρ_o is the mean seawater density, p is the pressure, $\mathbf{u}$ is the horizontal velocity vector, w is the vertical velocity, A_H is the horizontal viscosity, and K_v is the vertical viscosity. The terms on the right-hand side of 1 and 2 are Coriolis (*cor*), pressure gradient (*prsgrd*), horizontal and vertical advection (*hadv and vadv*), horizontal viscosity (*hvisc*) and vertical viscosity (*vvisc*). At 69°W, the interaction of the mesoscale flows results in flow confluence (Figure 7e) and alters the local pressure gradient (Figure 8c). The mean along-shelf sea level tilt

on the Northwest Atlantic shelf is in the range of $\sim 10^{-8}$ to 10^{-7}, based on observational inference and models with varying complexity (Chen & He, 2015; Lentz, 2008a; Scott & Csanady, 1976; Stommel & Leetmaa, 1972; Xu & Oey, 2011; Yang & Chen, 2021). Assuming constant along-shelf density of 1,025 kg m^{-3}, the sea level tilt of 10^{-8} to 10^{-7} yields an along-shelf pressure gradient term of $\sim 10^{-7}$ to 10^{-6} m s^{-2}. This range of the mean pressure gradient is much smaller than the local pressure gradient associated with the cyclonic circulation at 69°W, which is $\sim O(10^{-5}$ m $s^{-2})$ (Figure 8c). However, this negative local pressure gradient, that is, higher pressure eastward/poleward, is achieved in the presence of a strong along-shelf density gradient (Figure 8), which works against the pressure gradient setup. Using a depth-averaged along-shelf density gradient of 0.2 kg m^{-3} over 20 km at 69°W, the baroclinic portion of the pressure gradient due to the density gradient is estimated to be $\sim 10^{-5}$ m s^{-2} in the opposite direction to the total pressure gradient in Figure 8c. Therefore, the actual barotropic portion of the pressure gradient is larger than the baroclinic portion and the total pressure gradient. This scaling estimate is consistent with the depth structure of the pressure gradient, which is largely uniform through the water column suggesting barotropic dominance (Figure 8c). Indeed, the along-isobath sea surface height (i.e., total sea surface height in the model) has a large gradient, 0.07 m over 34 km, or $\sim 2 \times 10^{-6}$ (Figure 8g), much larger than the mean tilt. Similar local pressure gradient setup can be found at the other two sites of onshore intrusions between 71.5°W and 71°W and between 70°W and 69.4°W. The distinction is that the pressure gradient setup between 70°W and 69.4°W is predominantly baroclinic, that is, along-isobath density gradients rather than the sea surface tilt set up the negative pressure gradient. Nevertheless, for all three cases, the negative pressure gradient (higher pressure poleward) seems to be associated with the leading edge of the cyclonic eddies (Figure 7e), and is largely balanced by the Coriolis force with the onshore flows. The ageostrophic term (*ageo*, Figure 8d) is defined as the sum of Coriolis and pressure gradient terms on the right-hand side of Equation 2, that is,

$$ageo = cor + prsgrd = -f(u_g + u_a) - \frac{1}{\rho_o}\frac{\partial p}{\partial y} \tag{3}$$

Where u_g (u_a) is the geostrophic (ageostrophic) component of the cross-shelf flow. So, the ageostrophic cross-shelf velocity u_a can be retrieved as $ageo/(-f)$. The onshore intrusions at 69°W and to the east of 71.5°W are predominantly barotropic through the water column (Figure 8). The intrusion between 70°W and 69.4°W is subsurface-intensified, capped by offshore flow in the surface layer. This ageostrophic offshore flow is primarily driven by offshore Ekman transport (Figures 7a and 8f) with contributions from nonlinear momentum advection. It is worth noting that the ageostrophic velocity contributes a non-negligible portion of the total onshore flow, particularly in the interior of the water column (Figure 8d). While the three-layer structure of the ageostrophic circulation is similar to the structure of the mean cross-shelf flow (cf. Figure 2 in Lentz, 2008a), the momentum balance here is a significant departure from the mean state due to the elevated importance of ageostrophic processes associated with the cyclonic eddies.

It is useful to discuss the setup of the negative pressure gradient associated with the cyclonic eddies. The cyclonic circulation when either interacting with the equatorward shelfbreak jet or other mesoscale flows (Figure 7) can produce flow confluence, which could lead to a higher sea level at the leading edge (northeast side) of the cyclonic circulation pattern. Because of the lower sea surface height in cyclonic eddies, the increased sea level at the leading edge would weaken the cross-shelf sea level and pressure gradient. In the meantime, the sea level increase at the leading edge together with the impingement of the cyclonic eddy will increase the along-isobath pressure gradient because of the lower sea level at the onshore flank of the cyclonic eddy. These conjectured processes are evidenced by the along-shelf sea surface gradient at the 100 m isobath. Around 69°W and between 71.5°W and 71°W, both at the leading edge of two cyclones, significant along-isobath sea level tilt is apparent (Figure 8g). Also, model diagnostics reveal that the cross-shelf pressure gradient is attenuated at the leading edge of the two cyclonic eddies and is strengthened along the onshore flank of the eddies (not shown). Both the enhanced along-isobath pressure gradient and attenuated cross-isobath pressure gradient setup by the cyclonic eddies favor the cross-isobath onshore flow at the leading edge (Figures 7 and 8).

The time scale of these onshore intrusions is O(10 days). While the Coriolis term reveals the exchange of water masses by both onshore and offshore flows (Figure 8b), the onshore and offshore flows are by no means symmetric. The interleaving transport and tracer fluxes do not cancel, and examination of the four-dimensional temperature and salinity fields confirms that the onshore intrusion of warm and salty waters have a persistent presence on the outer continental shelf, which can be longer than ~20 days. As discussed below, the frequent presence of the

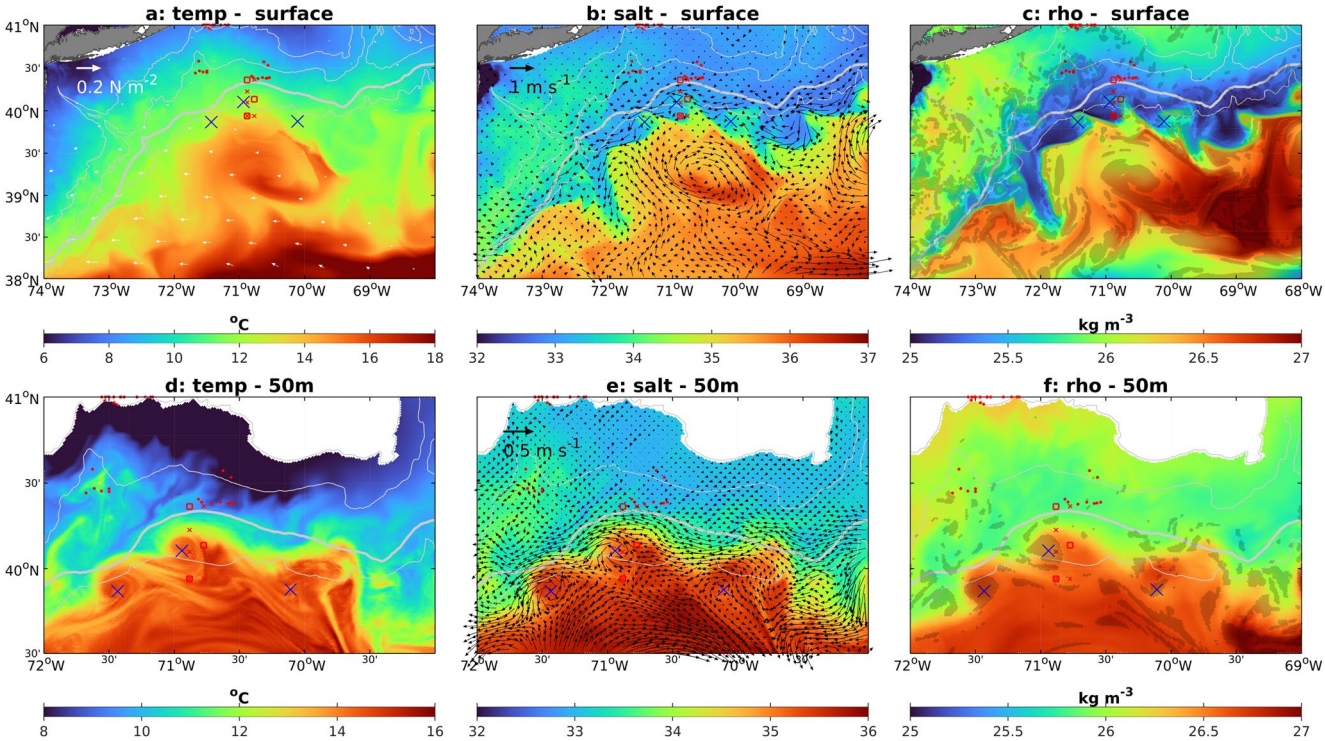

Figure 9. Model temperature (a), (d), salinity with subtidal currents (b), (e) and density with locations of relative vorticity larger than 0.3 *f* marked in shade (c), (f) on January 22, 2017. Panels (a–c): plane view at surface. Panels (d–f): plane view at 50 m. Wind stress vectors in white are overlaid in panel (a). All vectors are subsampled to aid visualization. 50, 70, 100, and 200-m isobaths are contoured in gray with 100 m isobath in thicker contour. Locations of CFRF/WHOI profiles and Pioneer Array mooring locations are also marked in red. Blue crosses denote the locations of cyclonic eddies.

WCRs, cyclonic eddies and the intrusions, and the persistence of the intruded water masses all work collectively to precondition the outer continental shelf for subsequent cross-shelf exchange.

The second period of intense shelfbreak exchanges is in the latter half of January 2017. The cyclonic eddy to the south of the southern New England shelfbreak in early-mid January 2017 (Figure 12b) eventually drifted out of the region and was displaced by the WCR later in the month (Figure 9). In the meantime, smaller scale cyclonic eddies developed at the onshore flank of the WCR, presumably resulting from the frontal instabilities and the interactions of the flow field. The eddies persisted for about 10 days, going through significant deformation and onshore extension (Section 3.3). The translation direction of these eddies is equatorward, or cyclonically, in the direction of the shelfbreak jet and in opposition to the rotation of the WCR. This is the opposite direction to that of the cyclonic eddies observed during the Warm Core Ring Program, which did rotate in the sense of the WCR (Joyce, 1984; Kennelly et al., 1985). This difference suggests that these small-scale cyclonic eddies after their formation do not always interact with the anticyclonic circulation at the periphery of the WCR. Instead, their trajectory may be controlled by the equatorward shelfbreak jet, which is consistent with the closer proximity of these eddies to the outer shelf in comparison to the cyclonic eddies in November (Figure 7).

Despite the differences between the cyclonic features in the two periods, the major momentum balance governing the onshore intrusions appears to be similar. Associated with the three cyclonic eddies near 70°W and 71.5°W, negative along-shelf pressure gradient at the leading edge can be clearly identified (Figure 10). The negative pressure gradient is clearly set up by the along-isobath sea surface tilt, which outweighs the baroclinic contribution associated with local density gradient. Because of cyclonic eddy near 70°W does not immediately impinge the 100 m isobath, pressure gradient setup at this location is not identifiable. Nevertheless, the negative pressure gradient at 70°W and 71.5°W drives onshore flow, which is largely geostrophic as the ageostrophic contribution is smaller than that in the first period and is more localized. The wind forcing is much weaker on January 15, 2017, and the weaker and localized ageostrophic flow is mainly contributed by the nonlinear advection, whereas wind forcing drives a significant portion of the ageostrophic cross-shelf flow on November 13, 2016.

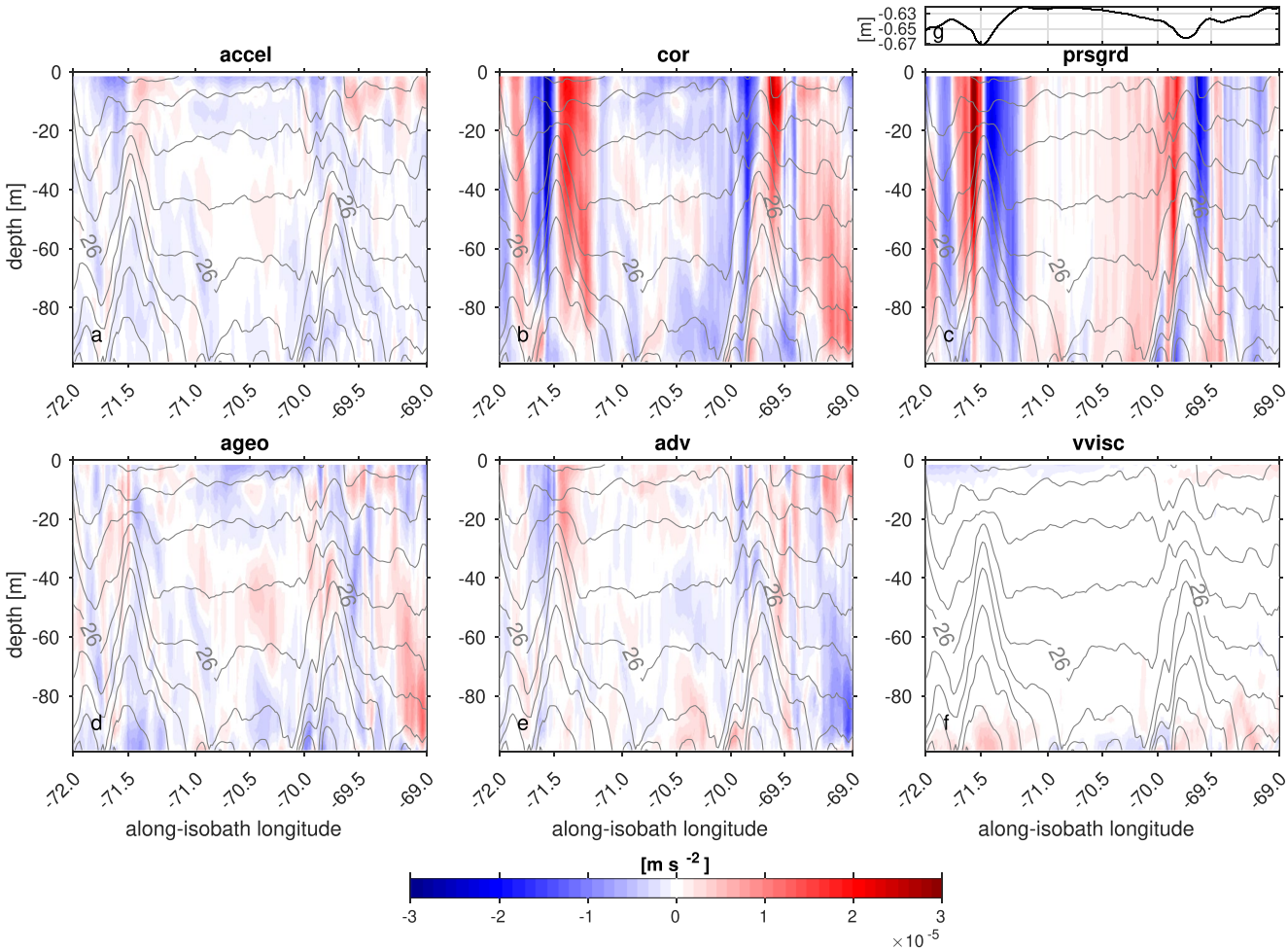

Figure 10. Along-isobath momentum balance at 100 m isobath on January 22, 2017: (a) acceleration (*accel*), (b) Coriolis (*cor*), (c) pressure gradient (*prsgrd*), (d) ageostrophic (*ageo*), (e) advection (*adv*), and (f) vertical viscosity (*vvisc*) terms. Density field is contoured in gray with contour interval 0.2 kg m^{-3}. Along-isobath sea surface height is plotted in panel (g). Negative pressure gradient means higher pressure poleward. Positive Coriolis term means onshore flow.

The width of the intrusions in January 2017 ranges from ~10 km during initiation to ~50 km in the later stage under the influence of strong wind forcing (Section 3.3). These scales are comparable to those in November 2016 and the baroclinic Rossby radius of deformation. The persistence of these intrusions is ~5 days, accompanied by downfront (in the direction of the frontal flow, equatorward) propagation of the warm/salty limbs (Figure 11). The onshore flows are largely geostrophic, although ageostrophic terms have a non-negligible contribution. The ageostrophic cross-shelf flows are primarily modulated by wind-driven processes. For example, the offshore (negative) ageostrophic currents (Figure 11) in the middle of the water column on 23 January are during a period of strong downfront wind, which accelerates the equatorward shelf flow, and drives onshore flow in the surface and offshore flow in the subsurface. Toward the end of January 2017, the downfront propagation of the intrusions stagnated presumably due to strong and persistent upwelling favorable wind (Figure 11 and Section 3.3) blowing against the along-shelf propagation of the intrusions.

3.2.2. Frontogenesis and Subsurface Intrusions

The shelfbreak front at the edge of the continental shelf in the Northwest Atlantic separates the cold, fresh, and light shelf water from the warm, salty, and dense slope water, supporting a baroclinic shelfbreak jet running equatorward (Fratantoni & Pickart, 2007; Linder & Gawarkiewicz, 1998). The impingement of cyclonic eddies results in the doming of the isopycnals which enhances the density gradient across the retrograde (isopleth slopes in opposite direction of the topography, i.e., sloping upward offshore) shelfbreak front and the flow at the onshore edge of the cyclonic eddy is in the same direction of the shelfbreak jet. These two factors sharpen the shelfbreak front

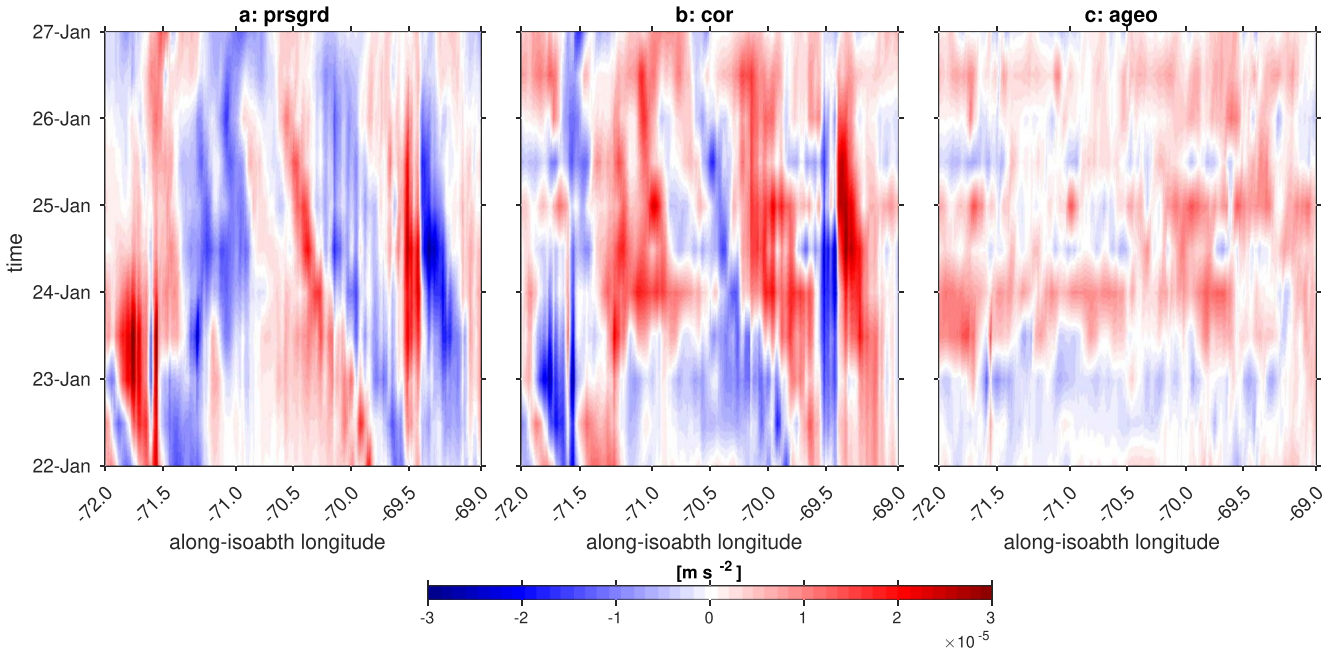

Figure 11. Temporal evolution of terms in the along-shelf momentum balance at 50 m along the 100 m isobath: (a) Pressure gradient *prsgrd*, (b) Coriolis *cor*, and (c) Ageostrophic *ageo*.

and induce secondary circulation in the vertical plane, that is, frontogenesis. The dynamical processes associated with frontogenesis and secondary circulation can be described using semi-geostrophic theory (Hoskins, 1982; Hoskins & Bretherton, 1972; Spall, 1995) in simple 2D settings, although deviations from semi-geostrophy should be considered for higher-order accuracy (e.g., McWilliams, 2021). Assuming that the shelfbreak jet is in geostrophic balance and the mixing terms are small in the along-shelf momentum balance Equation 2, the acceleration of the jet must be accompanied by cross-front movement, that is, $Dv_g/Dt = -fu_a$. In the meantime, the acceleration of the jet would increase the magnitudes of positive/negative vorticity seaward/shoreward of the front. Conservation of potential vorticity would require stretching/downwelling at the offshore side, and squashing/upwelling at the inshore side. Together, a secondary circulation would develop to satisfy mass conservation so that in the subsurface the flow goes from the offshore side to the inshore side, which may act as a potentially important mechanism for subsurface slope water intrusion.

Signs of frontogenesis and secondary circulation can be identified during both periods of intrusions associated with cyclonic eddies. In early November 2016 when the cyclonic eddy at 71.5°W was in close proximity to the shelfbreak, sharpening of the existing shelfbreak front is evident (Figures 12 and 13).The horizontal buoyancy gradient $|\nabla b| = \sqrt{b_x + b_y}$, where $b = -g\rho/\rho_0$, reveals intermittent yet strong fronts along the shelfbreak and the periphery of the cyclonic eddies. Along one cross-shelf transect at 72°W, the onshore flank of the cyclonic eddy interacted with the shelfbreak frontal system. The equatorward surface intensified shelfbreak jet was joined by the deep-reaching equatorward flow of the cyclonic eddy and the retrograde frontal isopycnals merged with the doming isopycnals of the eddy. The relative vorticity ζ/f (Rossby Number, Ro) is approaching 1 (Figure 13d), which is much larger than the observed values of the mean shelfbreak front at the New Jersey shelfbreak (Forsyth et al., 2020), as well as observed summertime and modeled mean shelfbreak front at the New England shelfbreak (Chen & He, 2010; Fratantoni et al., 2001). Frontal tendency, defined as the frontogenetical vector acting on the horizontal density gradient,

$$T_{adv} = \mathbf{Q_{adv}} \cdot \nabla_{\mathbf{h}}\rho = -(\rho_x u_x + \rho_y v_x, \rho_x u_y + \rho_y v_y) \cdot (\rho_x, \rho_y) \ldots\ldots \quad (4)$$

confirms the intensification of the shelfbreak front from surface to near bottom around the 100 m isobath (Figure 13e). Consistent with the sharpening of the shelfbreak front, secondary circulation develops (Figure 13f). Strong downward motion arises on the offshore side of the front, and onshore flow about 0.1 m s^{-1} occupies the lower half of the water column moving warm and salty water onshore. The temporal scale of the development of

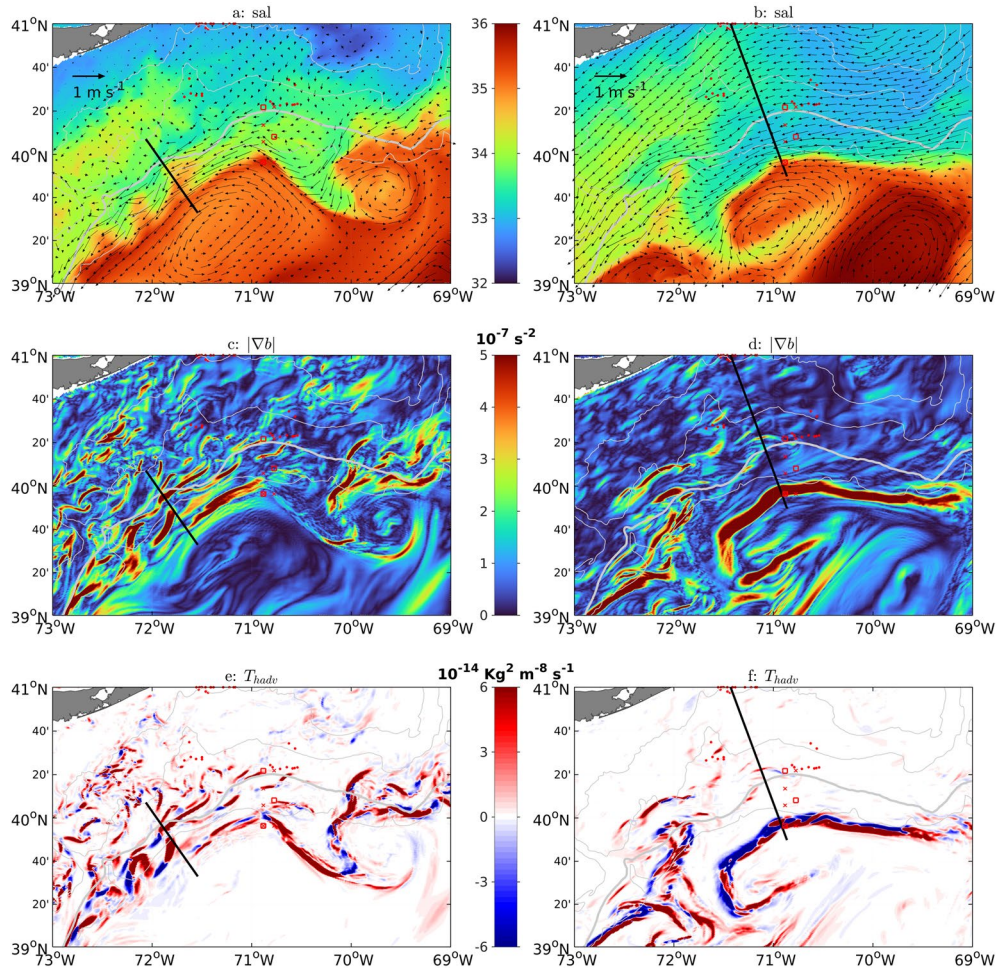

Figure 12. Surface salinity with currents (a), (b), frontal sharpness, that is, horizontal buoyancy gradient (c), (d), and frontal tendency by horizontal advection (e), (f) on 2016-11-10 (left panels, a, c, e) and 2017-01-08 (right panels, b, d, f). Vectors in panel (a and b) are subsampled for visualization purpose. 50, 70, 100, and 200 m isobaths are contoured in gray with 100 m isobath in thicker contour. The locations of 72W transect (Figure 13) and BI (Block Island) transect (Figure 14) are marked in panels (a) and (b) respectively.

the secondary circulation is O (1 day), which is not surprising considering the intermittent nature of frontogenesis (e.g., Capó et al., 2021; McWilliams, 2021).

Another example of frontogenesis and a subsurface onshore intrusion is in January 2017 when a cyclonic eddy interacted with a WCR at its offshore flank (Figure 12b and Figure 14). Along the onshore flank of the cyclonic eddy, along 200 m isobath at 40°N, strong horizontal buoyancy gradient developed as a result of the interaction of the cyclonic and the shelfbreak front and the confluent flow at the leading edges of the cyclonic eddy and the WCR. In this area, the onshore flow veers to align with the isobaths. It is worth pointing out that the horizontal buoyancy gradient around the WCR is not necessarily stronger than the gradient along the shelfbreak as the frontal sharpness could have been attenuated as the WCR crosses the slope sea. Along the 200 m isobath, the intensity of the shelfbreak front increases significantly. At 71°W where the cyclonic eddy was interacting with the shelfbreak jet, the Rossby number Ro is approaching 1.5 (Figure 14d), indicating strong nonlinear interaction in the submesoscale regime. Large tilt of the isopycnals and strong horizontal buoyancy gradients as well as intense frontal tendency are all consistent with frontogenesis (Figures 14a–14e). As the frontal tendency considered here accounts for the horizontal advection, the positive/negative tendency at the inshore/offshore side of the front suggests that in addition to the local intensification the shelfbreak front also moves onshore. This is confirmed by the secondary circulation in the cross-front plane (Figure 14f). Accompanied by the downward motion at the offshore side of the front, onshore flow in the middle water column is visible on the cyclonic eddy side. This suggests that

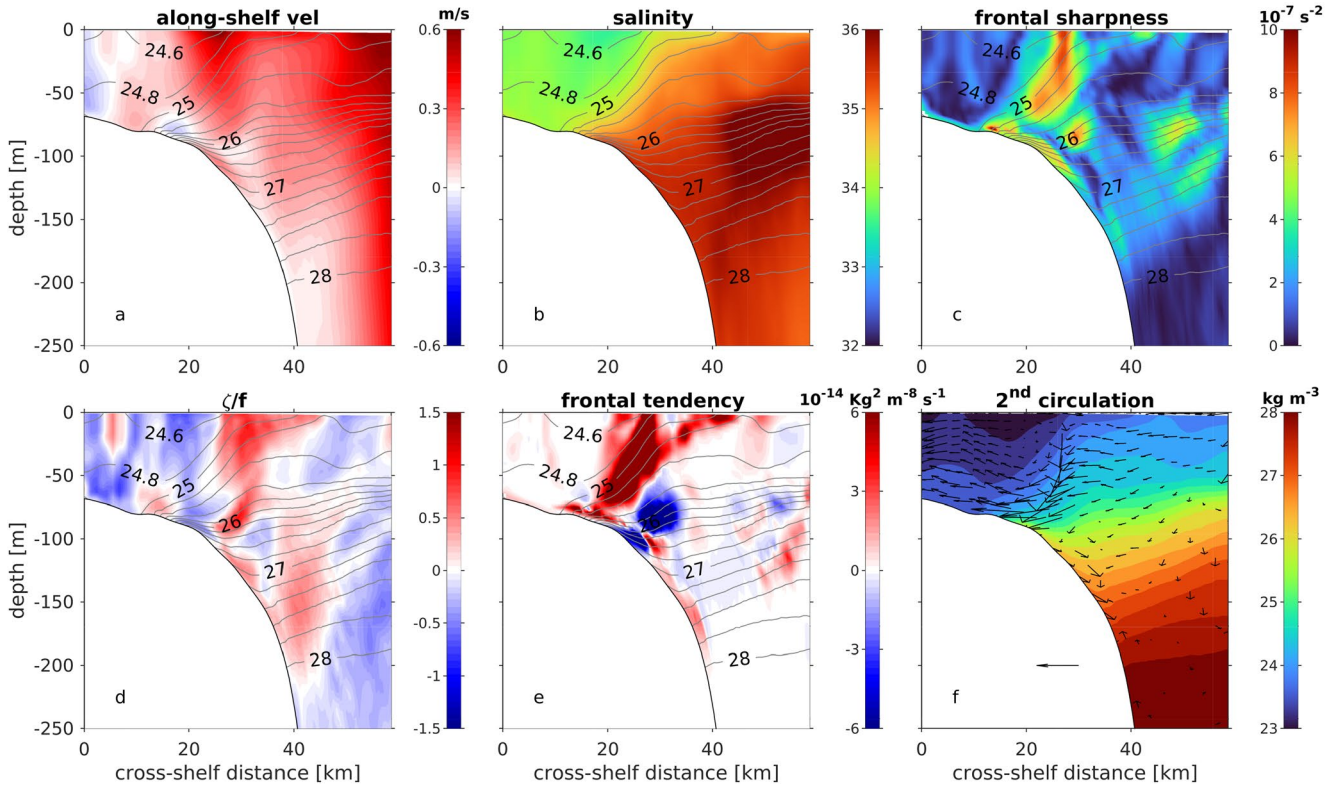

Figure 13. Cross-sectional view of frontal variables at the 72W transect (see Figure 12a for the location) on 2016-11-10 when a cyclonic eddy was immediately off the shelfbreak: along-shelf velocity (a, positive equatorward), salinity (b), frontal sharpness, that is, horizontal buoyancy gradient (c), relative vorticity scaled by Coriolis parameter (d), frontal tendency from horizontal strain (e), and secondary circulation (f). Density contours are shown in gray with a contour interval of 0.2 kg m^{-3}. Vertical velocity is scaled by 500. Horizontal velocity of 0.2 m s^{-1} is denoted in panel (f).

frontogenesis and secondary circulation in this oceanographic setting needs to consider both mesoscale straining by eddies and the translation of the mesoscale forcing. Consistent with the case in November 2016, the subsurface onshore flow can move far shoreward of the 100 m isobath before losing coherence (Figure 14f). Despite its intermittence, the secondary circulation can be a pathway of warm/salty slope water getting onto the outer continental shelf. The water mass anomaly can persist through diabatic, diapycnal processes, and precondition the outer shelf for further cross-shelf exchanges.

3.3. Cross-Shelf Penetration From the Outer Shelf

The two significant shelfbreak intrusion events in November 2016 and January 2017 are both associated with cyclonic eddies in close proximity to the shelfbreak. The difference, based on CFRF/WHOI Shelf Research Fleet profiles, is that the anomalies in water mass are more intense during January (Section 3.1). It was also in early January that anomalous water mass and Gulf Stream fish species were reported near Block Island (Figure 1), shallower than the 50 m isobath (Gawarkiewicz et al., 2019). Neither cyclonic eddies nor WCRs necessarily support penetration of slope water from the outer shelf all the way to the inner shelf as the exchange processes with these mesoscale eddies mainly occur at the outer shelf. Other ageostrophic processes must be active to move the anomalous water mass to the 50 m isobath and shallower regions. Examination of the NESS model and surface forcing shows that persistent and strong upwelling-favorable wind in late January 2017 effectively drove warm, salty slope water to the shallow regions near Block Island. Previous field studies such as Nantucket Shoals Flux Experiment (NSFE, Beardsley et al., 1985), Shelf Edge Exchange Program (SEEP-1, Houghton et al., 1988), and Coastal Mixing and Optics (CMO, Lentz et al., 2003) have discussed the importance of wind forcing in driving the cross-shelf migration of the foot of the shelfbreak front and the near-bottom temperature and salinity over the outer to middle shelf. The dynamical considerations have been based on a simple 2D wind-driven model (Boicourt & Hacker, 1976), that is, along-shelf wind sets up cross-shelf barotropic pressure gradient, which drives

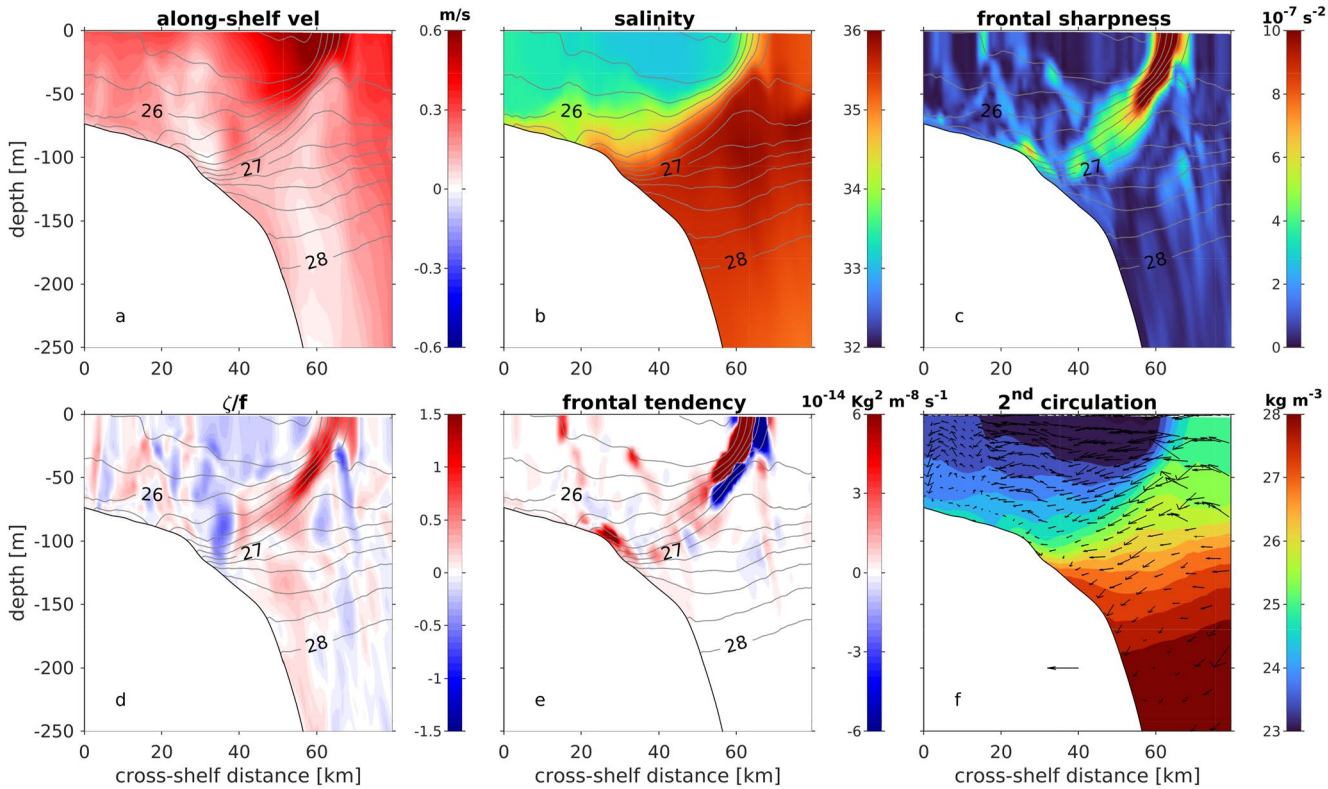

Figure 14. Cross-sectional view of frontal variables at the Block Island transect (see Figure 12b for the location) on 2017-01-08: along-shelf velocity (a, positive equatorward), salinity (b), frontal sharpness, that is, horizontal buoyancy gradient (c), relative vorticity scaled by Coriolis parameter (d), frontal tendency from horizontal strain (e), and secondary circulation (f). Density contours are shown in gray with a contour interval of 0.2 kg m^{-3}. Vertical velocity is scaled by 500. Horizontal velocity of 0.2 m m^{-3} is denoted in panel (f).

along-shelf current throughout the water column and the resulting bottom stress forces a cross-shelf bottom Ekman flow that moves the foot of the shelfbreak front in the cross-shelf direction. This 2D model largely explains the observed bottom salinity variability (at ~70.5°W) over the southern New England shelf during August 1996 to June 1997 (Lentz et al., 2003). However, the onshore penetration of water mass anomaly discussed below is similar but certainly different from the results in these previous studies.

The annual mean wind in the region is southeastward, with the mean wind stress O(0.02 N m^{-2}) (Lentz, 2008b). While the wintertime wind is also southeastward, the magnitude of the wintertime wind stress is larger, O(0.2 N m^{-2}) (Yang & Chen, 2021). The wind stress in late January 2017 was consistently strong, exceeding 0.2 N m^{-2} and lasting from January 26 to at least January 31 (Figure 15). Importantly, the wind was blowing to the east roughly in the along-shelf direction, that is, upwelling favorable, which consequently drives significant cross-shelf penetration (Figure 15). Because of the complex bathymetric features, the orientation of the isobaths, and the convoluted flow field, the intrusion takes the form of a salty and warm tongue. This distinctive feature began to develop at 71.5°W on January 26, gradually extending from the outer shelf toward the 50 m isobath. The width of the fully developed tongue-shaped intrusion was ~30 km, and was bottom intensified (Figure 16). The vertical scale of the intrusion is O(10 m), with a high-salinity, high-temperature core spreading across the sloping bottom. Within 6 days, the leading edge of the intrusion extended from ~100 m isobath to ~60 m isobath, a horizontal distance of ~100 km. This gives an estimated advective speed of ~0.2 m/s, which is generally larger than the onshore component of the secondary circulation at the shelfbreak front (Figures 13 and 14), and is even comparable to the speed of the mean shelfbreak jet (Chen & He, 2010; Fratantoni & Pickart, 2007; Linder & Gawarkiewicz, 1998; Zhang et al., 2011). Although the water mass anomalies are enhanced at the bottom and the intrusion is mainly isopycnal, the intrusion would certainly impact the hydrography of the whole water column due to diapycnal mixing and strong atmospheric forcing in winter (Figure 16).

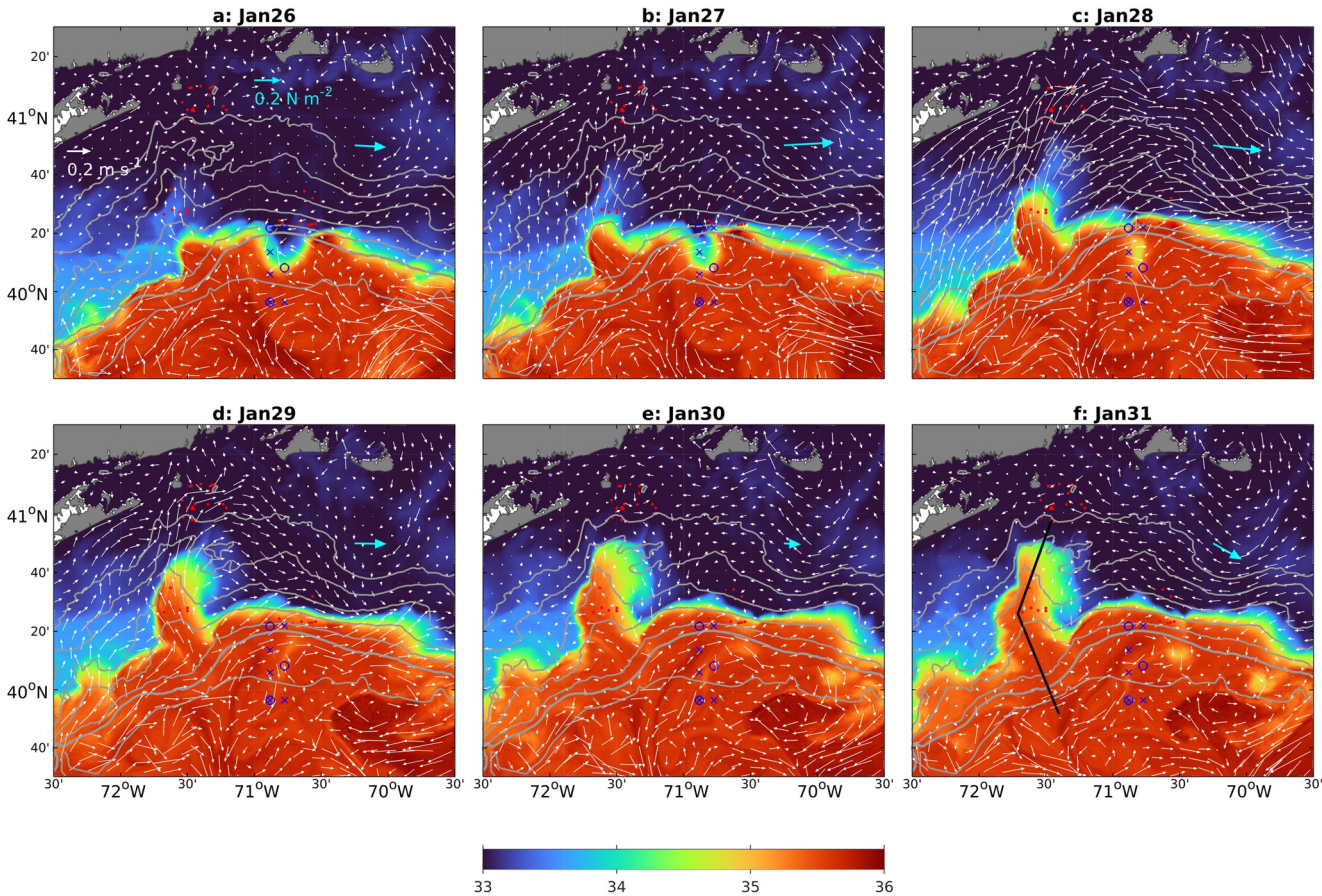

Figure 15. Evolution of subsurface salinity field (color) at the Southern New England shelf during January 26 to 31, 2017. Salinity at 100 m (off the shelfbreak) and along the sloping bottom (shoreward of 100 m isobath) is shown. White vectors represent the velocity field (subsampled every eight grid points) and cyan arrow denotes spatially averaged wind stress. 50, 60, 70, 80, 90, 100, and 200 m isobaths are contoured in gray with 100 m isobath in thicker contour. CFRF profiles are marked by red dots and Pioneer Array mooring locations are marked in blue with cross representing profiling moorings. One cross-shelf section slicing through the intruding salty water is shown in black in panel (f).

The cross-shelf bottom velocity suggests that the intrusion is locally intensified at 71W, roughly following a bathymetric trough at the mid-shelf (70 m isobath). Momentum diagnostics indicate that the major balance is between the pressure gradient force and the Coriolis term, that is, the setup of the pressure gradient drives the cross-shelf penetration. Indeed, an elevated pressure gradient is evident along the pathway of the intrusion from January 26 to 29, with high pressure to the right of the tongue-shaped intrusion (Figure 17). This is consistent with the enhanced cross-shelf velocity along the bottom during the same period (Figure 15), suggesting that the onshore penetration is largely geostrophic. The tongue-shaped pattern associated with the onshore velocity does not coherently show up in the ageostrophic vectors or other terms in the momentum balance including bottom friction (not shown). In the last two days of January 2017, the pressure gradient setup along the path of the intrusion gradually dissipates, corresponding to the disappearance of the onshore flow at the bottom. However, the advected anomalous water mass occupies a considerable portion of the shelf and has lasting impacts on the shelf hydrography.

The localized pressure gradient setup driving the onshore intrusion is worthy of discussion. Throughout the event, the wind is roughly parallel to the local isobaths to the east of ~71.5°W and has an along-isobath component to the west of 71.5° W, although the isobaths curve to the south. The resulting pressure gradient setup would be generally pointing onshore following the curvature of the isobaths (e.g., Figure 17b). Because of the changing orientation of the isobaths, the offshore point at ~71.5°W would have larger barotropic pressure due to the convergence of surface Ekman transport. Additionally, the cross-shelf component of the wind to the west of 71.5°W drives along-shelf Ekman transport equatorward, which would contribute to mass divergence and an enhanced

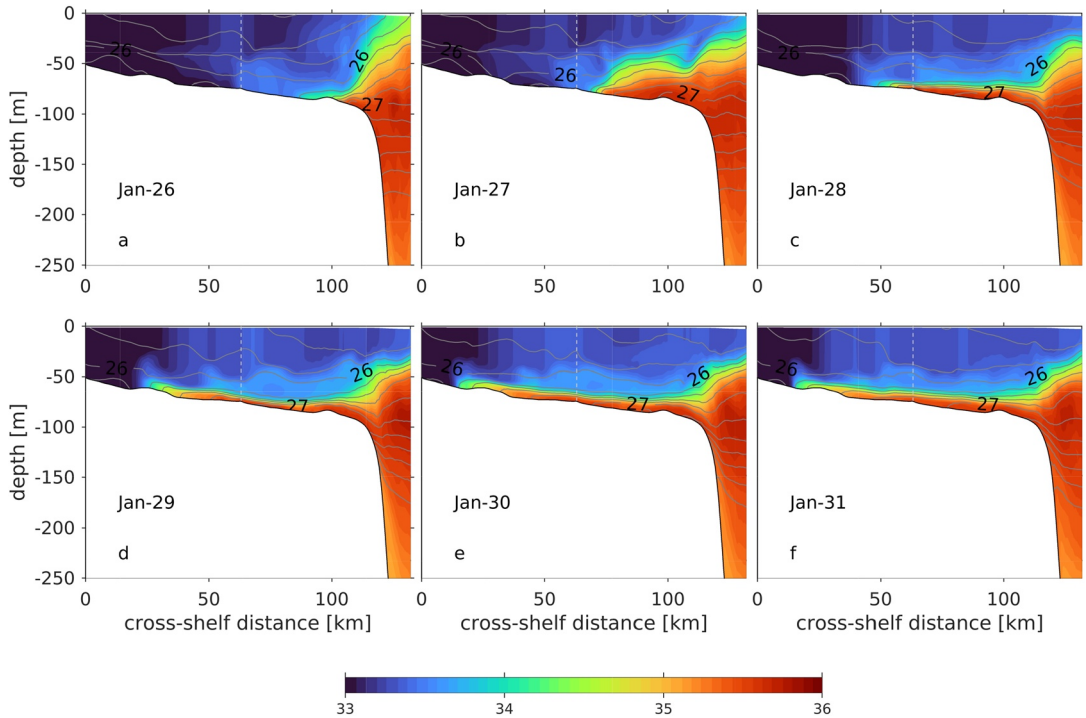

Figure 16. Bottom intensified intrusion as revealed by the evolution of the salinity field (color) along the cross-section in Figure 15f. Density field is in gray contours at an interval 0.2 kg m^{-3}. The vertical dashed line represents the turning point of the transect (Figure 15f).

barotropic pressure gradient setup around 71.5° W. Although other processes including baroclinic pressure gradient setup and flow convergence by non-wind-driven processes make it not always straightforward to pinpoint the exact causal factors for the particular pressure gradient driving the cross-shelf flow, along- and cross-isobath momentum balance at the 70m isobath in the path of the intrusion provides insight into the wind-driven process (Figure 18). As the upwelling-favorable wind persists from January 26, the bottom along-isobath pressure gradient increases at the curvature of the 70 m isobath (Figure 18a), although at other locations of the same isobath the cross-isobath pressure gradient term is more prominent (Figure 17). The difference is associated with the bathymetric feature of the trough where local isobaths veer from the along-shelf direction to the cross-shelf direction, particularly at the 70 m isobath. This local along-isobath pressure gradient drives an onshore geostrophic flow crossing the isobath at the bottom and is balanced by bottom friction exerting on the equatorward along-isobath flow locally (Figure 18a). In comparison, the cross-isobath pressure gradient is smaller and fluctuating despite the consistent bottom intrusion during January 26 to 29 (Figure 18b). The positive bottom friction in the cross-isobath direction is consistent with onshore bottom intrusion and is partially balanced by the Coriolis term, which is a result of equatorward along-isobath flow at this location. As the wind relaxes on January 30 and 31, the above terms gradually weaken and change direction, corresponding to the disappearance of the bottom intrusion.

The locally intensified bottom intrusion is distinctive from the results in previous work that treat the wind-driven cross-shelf exchange in a 2D fashion. While the broad-scale onshore pressure gradient and along-shelf flow in the direction of the upwelling-favorable wind are consistent with the conceptual wind-driven model (Boicourt & Hacker, 1976), the orientation of isobaths and local bathymetric features strongly determines the spatial variability of the bottom intrusion. The intensified bottom intrusion near 71.5°W on top of the general onshore migration of the location of the maximum salinity gradient, that is, the foot of the shelfbreak front (Figure 15) suggests that consideration of three dimensionality of the processes including the along-shelf change of bathymetry is essential for a comprehensive understanding of the wind-driven shelfbreak exchange processes.

The bathymetric effect on wind-driven circulation discussed here is different from the dynamical setting in the Hudson Shelf Valley where the cross-shelf (along-valley) pressure gradient drives cross-shelf (along-valley) flow in the valley as there is no along-shelf flow in the valley, that is, no cross-shelf Coriolis force. This is probably because the Hudson Shelf Valley is a more pronounced bathymetric feature and bottom friction there is more

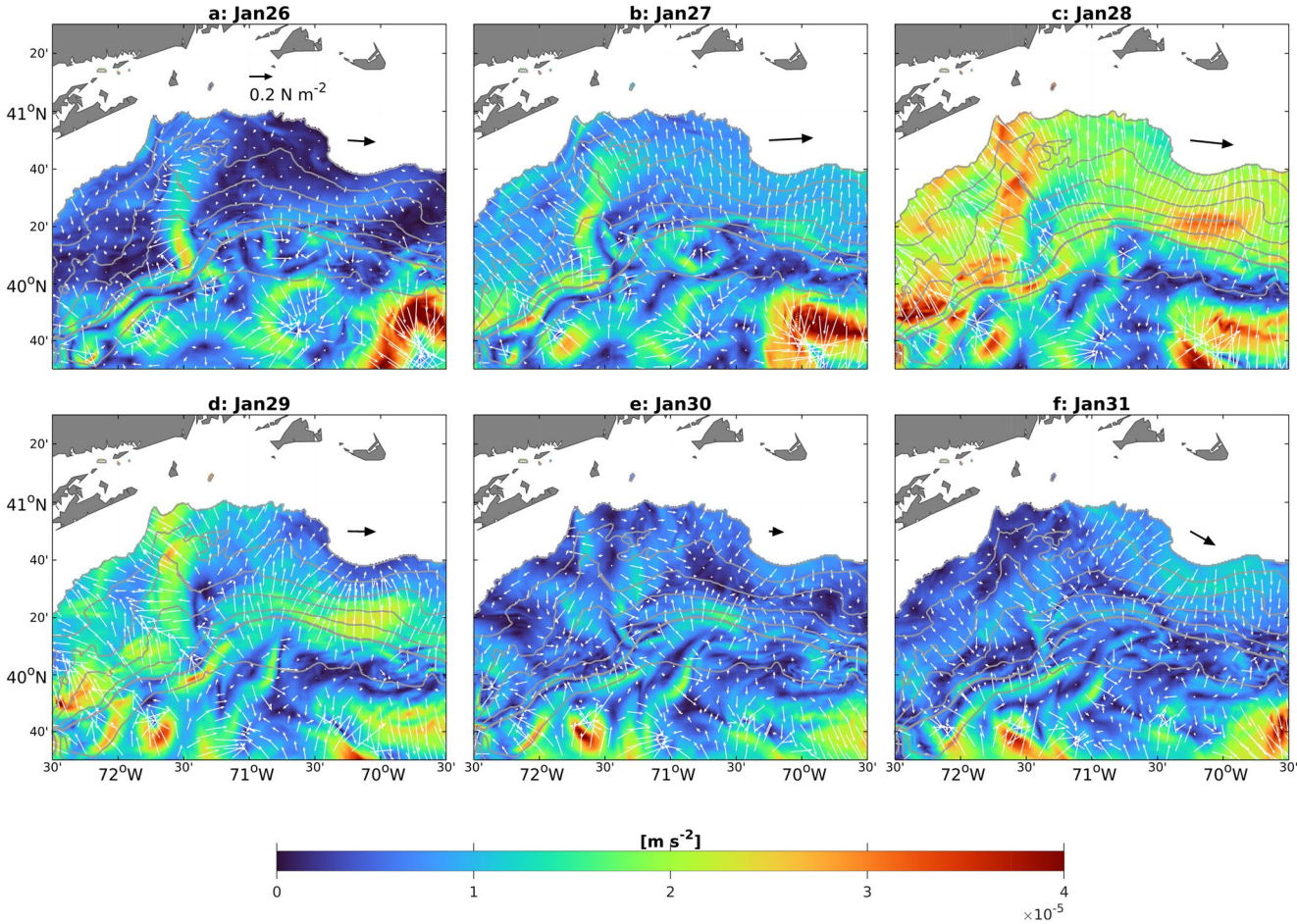

Figure 17. Pressure gradient force $\left(\frac{-1}{\rho_o}\nabla_H p\right)$ at 100 m (off the shelfbreak) and along the sloping bottom (shoreward of 100 m isobath). White vectors denote the direction of the pressure gradient. Spatially averaged wind stress is also shown in black vector in each panel. 50, 60, 70, 80, 90, 100, and 200 m isobaths are contoured in gray with 100 m isobath in thicker contour.

important (Lentz et al., 2014). Another similar setting in which bathymetric features play an important role in wind-driven circulation is the wintertime Yellow Sea, where the southward currents along the China and Korean coast are accompanied by the northward subsurface flow along the Yellow Sea Trough (Lin & Yang, 2011).

4. Discussion

4.1. Cyclonic Eddies

It is well known that between the Gulf Stream and the Northeast US continental shelf, WCRs can exert significant impact on shelfbreak exchange. The roles of other mesoscale features, for example, cyclonic eddies discussed above have received less attention, although their existence has long been realized (Churchill et al., 1986; Joyce, 1984; Kennelly et al., 1985). One reason may be the challenges in direct observations: current nadir altimetry products do not have enough resolution to capture these smaller scale features and SST imagery cannot necessarily resolve them either because of the attenuated thermal signature and uncertainties in inferring circulation based on SST alone. Shipboard and mobile platforms can certainly observe these eddies with small spatial and temporal scales, but coordinated sampling is required. For example, Pioneer Array offshore gliders survey the area off the shelfbreak, but they do not always sample at the right location and time. In addition, velocity measurement from mobile platforms is challenging (Todd et al., 2017). In the absence of dedicated observations, well-constructed primitive-equation models with realistic configuration can provide useful insights into the dynamics of these cyclonic eddies. There appears to be three types of cyclonic eddies discussed here. The

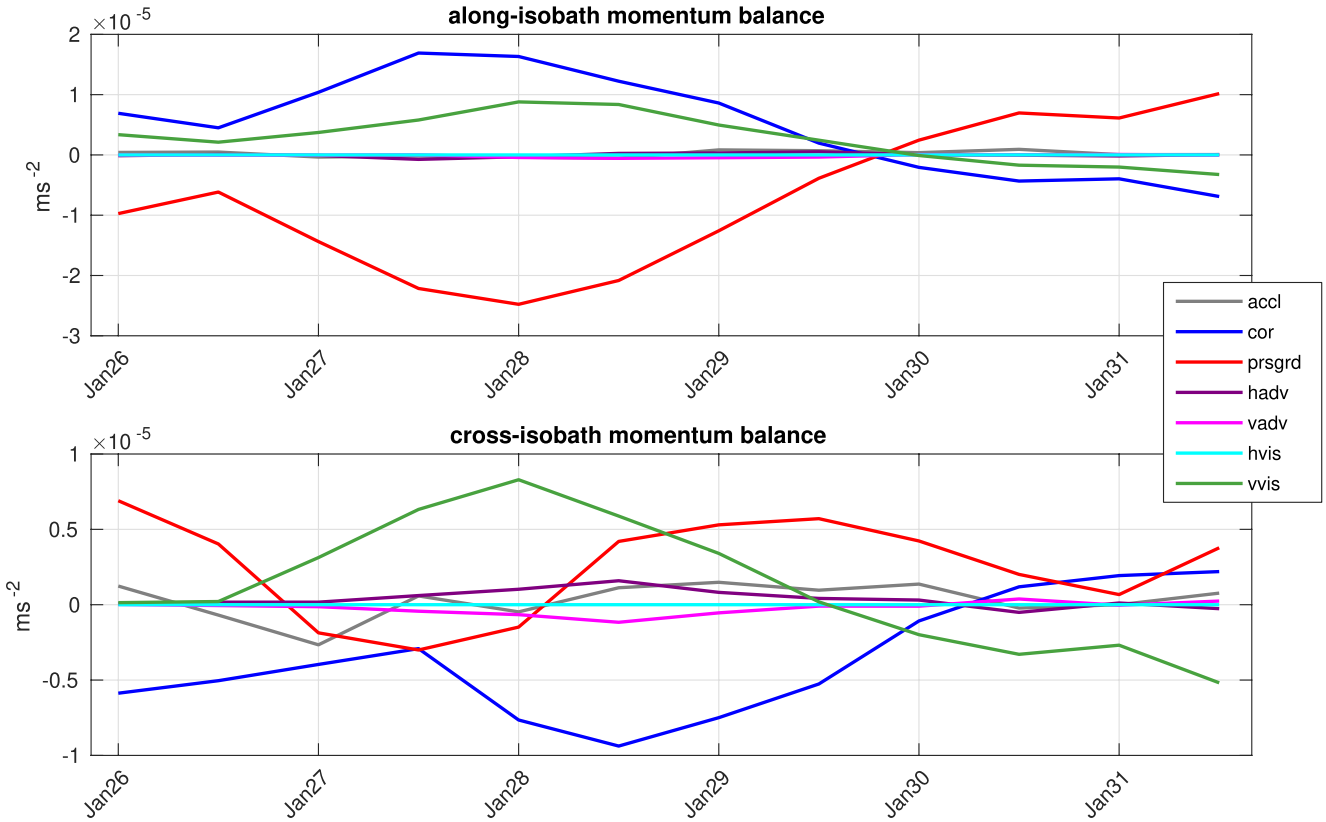

Figure 18. Along- and cross-isobath bottom momentum balance at the 70 m isobath in the path of the intrusion (thicker segment in Figure 17). The sign convention is consistent with the coordinate system in Figure 1, for example, negative pressure gradient term in the along-isobath balance means higher pressure poleward. Note the scale difference in the two panels.

frontogenetic cyclones (Figure 12) that are capable of intensifying the shelfbreak frontal system generally have slightly smaller horizontal scale but comparable vertical scale with WCRs, ~1,000–2,000 m. These cyclonic eddies are presumably the same type as the one observed by Churchill et al. (1986) and result from the interactions of the mesoscale flow field. Another type of cyclones has both smaller horizontal and vertical scales, 40–50 km in diameter, ~400–500 m, such as the one near 69.5°W on November 13, 2016 (Figure 7e). Because of the smaller vertical scale, these eddies can move closer to the shelfbreak in comparison to larger WCRs, which may be constrained by the bottom topography. As a result, the smaller cyclonic eddies can more directly interact with the shelfbreak front and the outer continental shelf, inducing significant shelfbreak exchange. The third type of cyclonic eddies appear to be at the frontal scale (Figure 9e), with a horizontal scale of ~20 km and a vertical scale of ~100 m. These eddies have a relatively shorter temporal scale of a few days, but can directly reside at the outer continental shelf interacting with the frontal circulation. Targeted field observations are necessary to provide a better understanding of these different types of cyclonic features.

4.2. Importance of Along-Shelf Representations

While exchanges of water masses between the coastal ocean and open ocean occur in the cross-shelf direction, representation of along-shelf processes should not be underestimated. As discussed above, the along-shelf variations of bathymetric features and topography play an intrinsic role in the wind-driven penetration of offshore water to the shallow regions. The along-shelf orientation of the isobaths also regulates the translation of the cyclonic eddies and thus can influence the interactions between the outer shelf and the eddies. For example, the incident angle of the cross-isobath flow associated with the cyclonic circulations is sensitive to the configuration of the local topography, which may diversify the extent and magnitude of cross-shelf intrusions. Another aspect is along-shelf propagation of cross-shelf intrusions of warm, salty slope water. Although high salinity water over the shelf can be almost certainly traced back to an offshore origin and is a better indicator for cross-shelf

exchanges, the salinity anomaly at one location alone may not necessarily differentiate whether the anomalous water mass is advected locally in the cross-shelf direction or whether the along-shelf advection of anomalies is initiated by cross-shelf exchanges upstream. One example is the salinity observations at the upstream inshore and central inshore sites of the Pioneer Array (Figure 4). Although salinity anomalies in November 2016 are more intense than those in January 2017 at these two locations, observations from CFRF/WHOI profiles suggest otherwise (Figure 3). The implication is that cross-shelf intrusions in November at the Pioneer Array did not reach shallower isobaths directly, whereas the intrusions in January did. In either case, along-shelf propagation of the intruded anomalies is well resolved in the model, which highlights the importance of realistic representation of along-shelf settings, for example, bathymetry and along-shelf variation of pressure gradient in resolving cross-shelf exchanges. In that sense, cross-shelf exchanges are inherently heterogeneous and future work is needed to unravel potential hotspots of enhanced cross-shelf exchanges. For example, anomalous warm and salty water was also found along a bathymetric channel close to the Block Island in the depth range of 30–50 m in late fall 2009 (Ullman et al., 2014). While the exact cause of this event is not entirely clear, impingement of a Gulf Stream warm-core ring at the shelfbreak and wind forcing appear to be responsible (Ullman et al., 2014). Whether or not a part of the southern New England shelf is a hotspot for cross-shelf exchange remains to be confirmed. Understanding of the spatial heterogeneity of cross-shelf exchange would contribute to the development of prediction skill of the shelf environment and is important for the management of marine resources and commercial fisheries.

4.3. Combined Cyclonic Eddy and Wind Forcing Effects on Shelfbreak Exchange

WCRs are frequently shed from the Gulf Stream and their active presence in the slope sea is not rare. Although multiple WCRs were in close proximity to the shelfbreak during November 2016 and February 2017, they did not significantly elevate the temperature near the shelfbreak. Examination of SST from both AVHRR OI SST and HYCOM/NCODA GOFS3.0 confirm that neither the average SST during November 2016 to February 2017 nor average SST in January 2017 in the slope sea off the southern New England shelfbreak was the highest during 1982–2018 (not shown), although they were on the warmer end. Additional analysis of HYCOM fields at 100 m off the shelfbreak during 1995–2017 does not suggest a dramatic deviation of subsurface temperature or salinity in January 2017 either. On the other hand, strong, persistent upwelling-favorable wind during wintertime is not uncommon. This is further confirmed by the analysis of January wind speed from 1993 to 2017 in ERA5: Both monthly-mean eastward wind speed and average eastward wind stronger than 10 m s^{-1} during January 2017 were on the stronger side, but neither was the strongest during 1993–2017. However, the preconditioning of the outer shelf associated with cyclonic eddies and WCRs and strong upwelling-favorable wind work jointly during the January intrusion. The shelfbreak exchange in late January was immediately followed by persistent upwelling-favorable winds, which makes a one-two combination that is more effective than either process alone in producing large-magnitude anomalies.

A similar bottom intrusion occurred in late November 2016 (Figure 19a), which also resulted from upwelling-favorable wind from November 20 to November 23 acting upon the preconditioned outer shelf. However, the wind magnitude was not as large and the wind direction was not as persistent as the conditions in late January 2017. As a result, the magnitude of the salinity anomaly and its onshore extent was not as dramatic (Figure 19a vs. Figure 15f). If, however, the wind condition from November 19 to 27, 2016 is replaced with that in January 24 to February 1, 2017, that is, stronger and more persistent upwelling-favorable wind, a more pronounced bottom intrusion results (Figure 19b). The tongue-shaped intrusion at 71.5°W in this experiment with stronger wind is qualitatively similar to the January 2017 intrusion. Because in both periods the outer shelf has been preconditioned by offshore eddies, the importance of preconditioning cannot be directly evaluated, although one can expect that an attenuated water mass anomaly at the outer shelf would unlikely produce a significant warm and salty intrusion. In comparison, the role of wind forcing is more definitive. An additional sensitivity experiment with no wind forcing during January 24 to February 1, 2017 shows that without strong and persistent upwelling-favorable wind, no bottom intrusion will occur in late January 2017 (Figure 19c).

The rapidly developing onshore intrusion in late January 2017 with strong upwelling-favorable winds highlights the importance of weather-band forcing in cross-shelf exchange. Future work is necessary to examine the long-term variability in the wind forcing and the impacts on cross-shelf exchanges in the context of long-term warming (Chen et al., 2020) and changing Gulf Stream behavior (Andres, 2016; Gangopadhyay et al., 2019).

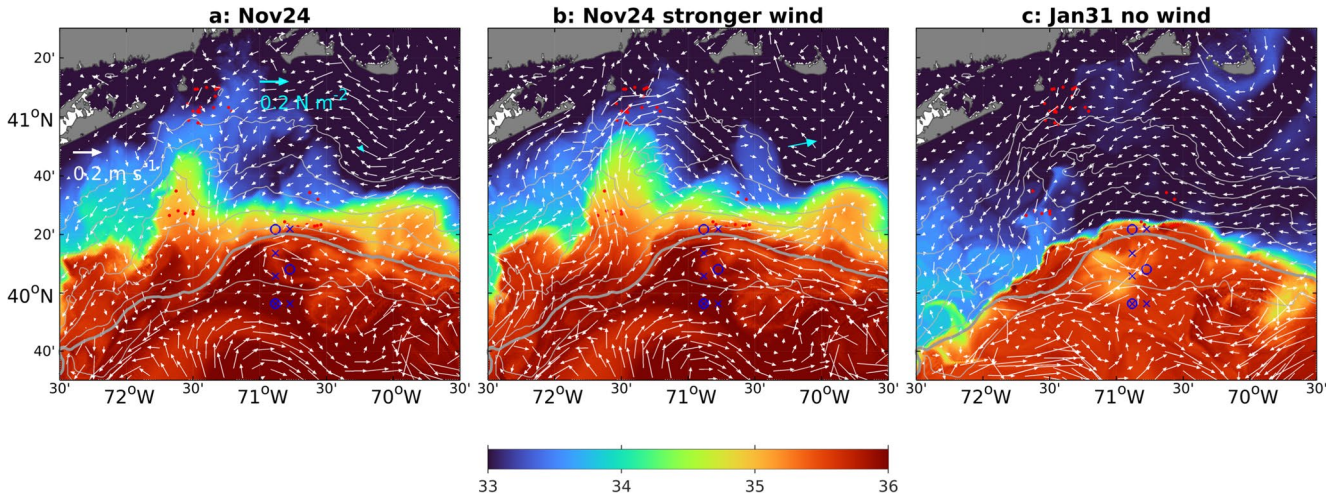

Figure 19. Subsurface salinity field showing a bottom intrusion in late November 2016 (a), an enhanced intrusion in late November 2016 with stronger wind (b), and no intrusion with no wind in late January 2017. Salinity at 100 m (off the shelfbreak) and along the sloping bottom (shoreward of 100 m isobath) is shown. White vectors represent the velocity field (subsampled every eight grid points) and cyan arrow denotes spatially averaged wind stress. 50, 60, 70, 80, 90, 100, and 200 m isobaths are contoured in gray with 100 m isobath in thicker contour. CFRF profiles are marked by red dots and Pioneer Array mooring locations are marked in blue with cross representing profiling moorings.

5. Summary

The Northwest Atlantic coastal ocean including the Northeast US continental shelf has been experiencing both enhanced long-term warming (e.g., Chen et al., 2020; Forsyth et al., 2015) and extreme temperature anomalies, that is, Marine Heatwaves (e.g., Chen, Gawarkiewicz, et al., 2014; Chen et al., 2015; Schlegel et al., 2021). A variety of observations reveal an advective Marine Heatwave over the continental shelf in the Middle Atlantic Bight (MAB) in early January 2017 (Gawarkiewicz et al., 2019), which forms over the southern New England shelf, translates along the MAB shelf, and decays and exits the shelf near Cape Hatteras. Because multiple Gulf Stream WCRs were present in the slope sea and because of the known importance of WCRs in shelf-ocean exchange, it was hypothesized that these WCRs drove the warm and salty slope water onto the continental shelf and initiated the water mass anomalies (Marine Heatwave). Due to the limitations of the existing observations, whether or not the WCRs indeed were able to drive onshore intrusions across a large distance and the dynamical processes underlying the large-magnitude anomalies were not investigated.

This study combines the available observations and a newly constructed 1-km high-resolution regional model to unravel the dynamics of the physical processes initiating this advective Marine Heatwave. Scrutiny of the model output confirms its skill and capability of capturing the observed water mass anomalies. The model fields reveal multiple processes working in combination to produce large-magnitude intrusions and water mass anomalies. The model prognostics indicate that cyclonic eddies, instead of anti-cyclonic WCRs, play an important role in shelf-break exchange. These cyclonic eddies are generated as a result of interactions of the mesoscale flow field associated with the WCRs and have smaller spatial scales of 10–50 km. The cyclonic circulation patterns influence the shelfbreak exchange in two ways. First, they can induce local pressure gradient changes in the along-isobath direction through flow confluence and sea level setup. As a result, the along-isobath pressure gradient is mainly barotropic and drives cross-shelf flows, which are largely geostrophic with some contributions from ageostrophic processes (Figures 8 and 10). This process is identified during the two periods of significant cross-shelf intrusions in November 2016 and January 2017. Second, the flow at the onshore flank of the cyclonic eddies is in the same direction as the equatorward shelfbreak jet, and the doming isopycnals in an eddy can effectively increase the buoyancy gradient across the shelfbreak front. Both processes provide favorable conditions for the intensification of the front, that is, frontogenesis, which is evident during both the November and January intrusions, when cyclonic eddies were in close proximity to the shelfbreak (Figures 12–14). The resulting secondary circulation in the cross-front plane opens up a pathway for offshore water to travel along isopycnals and reach the outer continental shelf before diapycnal processes dissipate the anomalous water mass. The time scale of pressure gradient induced intrusion is O(10 days) and subsurface intrusion by frontogenesis is O(1 day). Despite the short

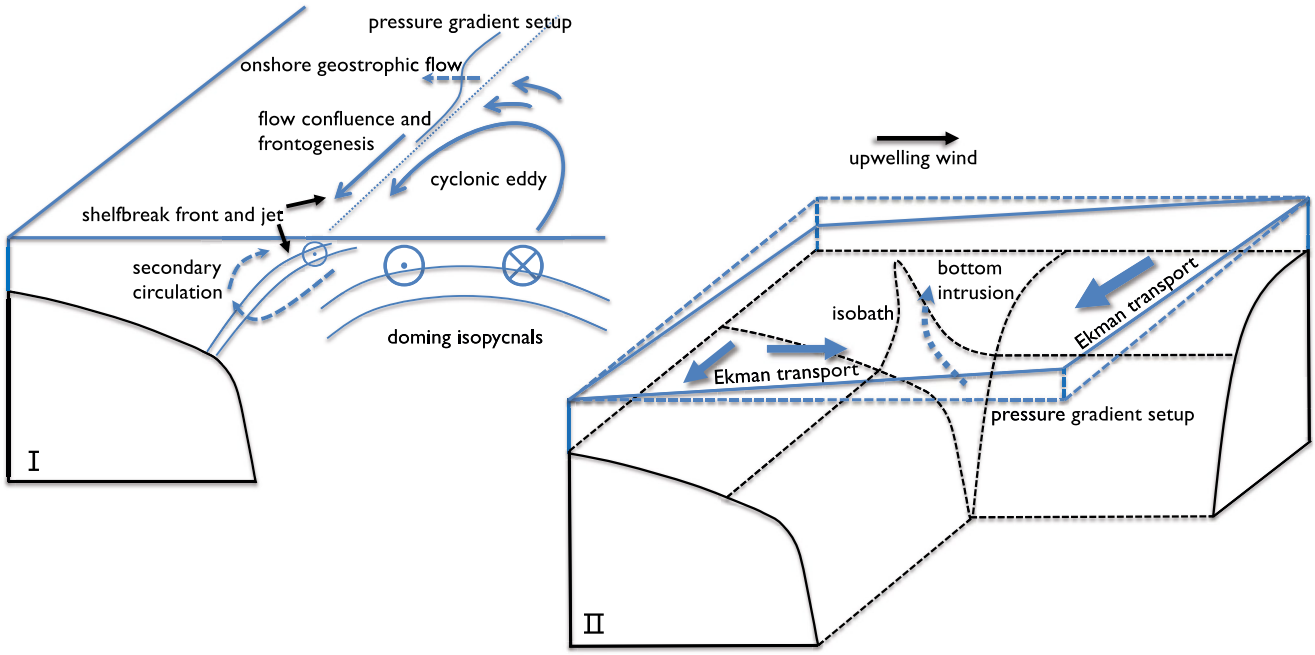

Figure 20. Schematic showing the one-two combination of cyclonic eddies and upwelling wind in producing large-magnitude temperature and salinity anomalies over the shelf.

time scale and intermittency, these two mechanisms work jointly to allow cross-isobath intrusions and preconditioning of the outer shelf. Following the cyclonic intrusions and preconditioning in late January 2017, strong and persistent upwelling-favorable wind sets up a local pressure gradient and drives rapid cross-shelf penetration of offshore water in the form of a bottom intensified warm/salty tongue. Within ~5 days, the warm/salty water travels 100 km onshore from the outer continental shelf, at a remarkable speed of ~0.2 m s^{-1}. Both the orientation of the isobaths and bathymetric features are intrinsic for the pressure gradient setup and onshore penetration, which implies the importance of realistic representation of along-shelf factors in understanding cross-shelf exchange.

The above cross-shelf exchange can be best described as a one-two combination of cyclonic eddies and upwelling-favorable winds (Figure 20). Although the hydrographic conditions off the shelfbreak are not particularly anomalous and the wind forcing is not particularly different from typical wintertime conditions, these two processes work jointly to drive the cross-shelf penetration over a significant onshore distance with large-magnitude temperature and salinity anomalies. The effectiveness of the combination hinges on the degree of synchronization of the processes. This probably explains why such significant cross-shelf exchanges are infrequent. The results presented here are consistent with the observations and reported unusual catch of Gulf Stream fish species in shallow waters (Gawarkiewicz et al., 2018). Furthermore, this study provides dynamical explanations of the observed water mass anomalies across the shelf, offers new insights about cross-shelf exchange during a time of changing oceanographic conditions, and lays the ground work for future studies looking into the manifestation at longer time scales and quantifying the contributions of these processes to regional water mass properties.

Data Availability Statement

Daily composite AVHRR SST is provided by Mid-Atlantic Regional Association Coastal Ocean Observing System (MARACOOS, http://tds.maracoos.org/thredds/REALTIME-SST.html). CFRF/WHOI Shelf Fleet data are available at http://science.whoi.edu/users/seasoar/cfrfwhoi/. OOI Pioneer Array data can be found at https://oceanobservatories.org/array/coastal-pioneer-array/. ERA5 reanalysis is available at https://www.ecmwf.int/en/forecasts/datasets/reanalysis-datasets/era5. HYCOM/NCODA output is available at https://www.hycom.org/dataserver/gofs-3pt0. Results presented in this study along with visualization codes are accessible at https://doi.org/10.5281/zenodo.5645415.

Acknowledgments
This work was supported by Woods Hole Oceanographic Institution (WHOI) Independent Research and Development (IR&D) award and National Oceanic and Atmospheric Administration (NOAA) Climate Program Office (CPO) Climate Variability and Predictability (CVP) program under grant NA20OAR4310398. Numerical modeling work was conducted at WHOI High-Performance Computing cluster Poseidon with startup support to Ke Chen. Comments and suggestions from Drs. Steve Lentz and Ken Brink on an early draft are greatly appreciated.

References

Andres, M. (2016). On the recent destabilization of the Gulf Stream path downstream of Cape Hatteras. *Geophysical Research Letters*, *43*, 9836–9842. https://doi.org/10.1002/2016gl069966

Bane, J. M., Brooks, D. A., & Lorenson, K. R. (1981). Synoptic observations of the three-dimensional structure and propagation of Gulf Stream meanders along the Carolina continental margin. *Journal of Geophysical Research*, *86*, 6411–6425. https://doi.org/10.1029/jc086ic07p06411

Beardsley, R. C., Chapman, D. C., Brink, K. H., Ramp, S. R., & Schlitz, R. (1985). The Nantucket Shoals Flux Experiment (NSFE79). Part 1, A basic description of the current and temperature variability. *Journal of Physical Oceanography*, *15*, 713–748. https://doi.org/10.1175/1520-0485(1985)015<0713:tnsfep>2.0.co;2

Benthuysen, J. A., Oliver, E. C. J., Chen, K., & Wernberg, T. (2020). Editorial: Advances in understanding marine heatwaves and their impacts. *Frontiers in Marine Science*, *7*. https://doi.org/10.3389/fmars.2020.00147

Boicourt, W. C., & Hacker, P. W. (1976). Circulation on the Atlantic continental shelf of the United States, Cape May to Cape Hatteras. In J. C. J. Nihoul (Ed.), *Memoires de la Societe Royale des Sciences de Liege* (pp. 187–200). University of Liege.

Brink, K. H. (2016). Cross-shelf exchange. *Annual Review of Marine Science*, *8*, 59–78. https://doi.org/10.1146/annurev-marine-010814-015717

Capó, E., McWilliams, J. C., Mason, E., & Orfila, A. (2021). Intermittent frontogenesis in the Alboran Sea. *Journal of Physical Oceanography*, *51*, 1417–1439.

Chapman, D. C. (1985). Numerical treatment of cross-shelf open boundaries in a barotropic coastal ocean model. *Journal of Physical Oceanography*, *15*, 1060–1075. https://doi.org/10.1175/1520-0485(1985)015<1060:ntocso>2.0.co;2

Chassignet, E. P., Hurlburt, H. E., Smedstad, O. M., Halliwell, G. R., Hogan, P. J., Wallcraft, A. J., et al. (2006). The HYCOM (HYbrid Coordinate Ocean Model) data assimilative system. *Journal of Marine Systems*, *65*, 60–83.

Chen, K., Gawarkiewicz, G., Kwon, Y.-O., & Zhang, W. G. (2015). The role of atmospheric forcing versus ocean advection during the extreme warming of the Northeast U.S. continental shelf in 2012. *Journal of Geophysical Research: Oceans*, *120*, 4324–4339. https://doi.org/10.1002/2014jc010547

Chen, K., Gawarkiewicz, G., & Plueddemann, A. J. (2018). Atmospheric and offshore forcing of temperature variability at the shelf break: Observations from the OOI Pioneer Array. *Oceanography*, *31*, 72–79. https://doi.org/10.5670/oceanog.2018.112

Chen, K., Gawarkiewicz, G. G., Lentz, S. J., & Bane, J. M. (2014). Diagnosing the warming of the Northeastern U.S. Coastal Ocean in 2012: A linkage between the atmospheric jet stream variability and ocean response. *Journal of Geophysical Research: Oceans*, *119*, 218–227. https://doi.org/10.1002/2013jc009393

Chen, K., & He, R. (2010). Numerical investigation of the middle atlantic bight shelfbreak frontal circulation using a high-resolution ocean hindcast model. *Journal of Physical Oceanography*, *40*, 949–964. https://doi.org/10.1175/2009jpo4262.1

Chen, K., & He, R. (2015). Mean circulation in the coastal ocean off northeastern North America from a regional-scale ocean model. *Ocean Science*, *11*, 503–517. https://doi.org/10.5194/os-11-503-2015

Chen, K., He, R., Powell, B. S., Gawarkiewicz, G. G., Moore, A. M., & Arango, H. G. (2014). Data assimilative modeling investigation of Gulf Stream Warm Core Ring interaction with continental shelf and slope circulation. *Journal of Geophysical Research: Oceans*, *119*, 5968–5991. https://doi.org/10.1002/2014jc009898

Chen, K., Kwon, Y.-O., & Gawarkiewicz, G. (2016). Interannual variability of winter-spring temperature in the Middle Atlantic Bight: Relative contributions of atmospheric and oceanic processes. *Journal of Geophysical Research: Oceans*, *121*, 4209–4227. https://doi.org/10.1002/2016jc011646

Chen, Z., Kwon, Y.-O., Chen, K., Fratantoni, P., Gawarkiewicz, G., & Joyce, T. M. (2020). Long-term SST variability on the northwest Atlantic Continental Shelf and slope. *Geophysical Research Letters*, *47*, e2019GL085455. https://doi.org/10.1029/2019gl085455

Cherian, D. A., & Brink, K. H. (2016). Offshore transport of shelf water by deep-ocean eddies. *Journal of Physical Oceanography*, *46*, 3599–3621. https://doi.org/10.1175/jpo-d-16-0085.1

Chin, T. M., Vazquez-Cuervo, J., & Armstrong, E. M. (2017). A multi-scale high-resolution analysis of global sea surface temperature. *Remote Sensing of Environment*, *200*, 154–169. https://doi.org/10.1016/j.rse.2017.07.029

Churchill, J. H., Cornillon, P. C., & Milkowski, G. W. (1986). A cyclonic eddy and shelf-slope exchange associated with a Gulf Stream warm-core ring. *Journal of Geophysical Research*, *91*, 9615–9623. https://doi.org/10.1029/jc091ic08p09615

Egbert, G. D., & Erofeeva, S. Y. (2002). Efficient inverse modeling of barotropic ocean tides. *Journal of Atmospheric and Oceanic Technology*, *19*, 183–204. https://doi.org/10.1175/1520-0426(2002)019<0183:eimobo>2.0.co;2

Fairall, C. W., Bradley, E. F., Hare, J. E., Grachev, A. A., & Edson, J. B. (2003). Bulk parameterization of air–sea fluxes: Updates and verification for the COARE algorithm. *Journal of Climate*, *16*, 571–591. https://doi.org/10.1175/1520-0442(2003)016<0571:bpoasf>2.0.co;2

Flagg, C. N., Dunn, M., Wang, D., Rossby, H. T., & Benway, R. L. (2006). A study of the currents of the outer shelf and slope from a decade of shipboard ADCP observations in the Middle Atlantic Bight. *Journal of Geophysical Research*, *111*. https://doi.org/10.1029/2005JC003116

Flierl, G. R., Stern, M. E., & Whitehead, J. A. (1983). The physical significance of modons: Laboratory experiments and general integral constraints. *Dynamics of Atmospheres and Oceans*, *7*, 233–263. https://doi.org/10.1016/0377-0265(83)90007-6

Forsyth, J., Andres, M., & Gawarkiewicz, G. (2015). Recent accelerated warming of the continental shelf off New Jersey: Observations from the CMV Oleander expendable bathythermograph line. *Journal of Geophysical Research: Oceans*, *120*, 2370–2384. https://doi.org/10.1002/2014jc010516

Forsyth, J., Andres, M., & Gawarkiewicz, G. (2020). Shelfbreak jet structure and variability off New Jersey using ship of opportunity data from the CMV oleander. *Journal of Geophysical Research: Oceans*, *125*, e2020JC016455. https://doi.org/10.1029/2020jc016455

Fratantoni, P. S., & Pickart, R. S. (2007). The Western North Atlantic Shelfbreak current system in summer. *Journal of Physical Oceanography*, *37*, 2509–2533. https://doi.org/10.1175/jpo3123.1

Fratantoni, P. S., Pickart, R. S., Torres, D. J., & Scotti, A. (2001). Mean structure and dynamics of the Shelfbreak jet in the Middle Atlantic bight during fall and winter. *Journal of Physical Oceanography*, *31*, 2135–2156. https://doi.org/10.1175/1520-0485(2001)031<2135:msadot>2.0.co;2

Gangopadhyay, A., Gawarkiewicz, G., Silva, E. N. S., Monim, M., & Clark, J. (2019). An observed regime shift in the formation of warm core rings from the Gulf Stream. *Scientific Reports*, *9*, 12319. https://doi.org/10.1038/s41598-019-48661-9

Garfield, N., & Evans, D. L. (1987). Shelf water entrainment by Gulf Stream warm-core rings. *Journal of Geophysical Research*, *92*(13), 3–13. https://doi.org/10.1029/jc092ic12p13003

Gawarkiewicz, G., Chen, K., Forsyth, J., Bahr, F., Mercer, A. M., Ellertson, A., et al. (2019). Characteristics of an advective marine heatwave in the Middle Atlantic Bight in early 2017. *Frontiers in Marine Science*, *6*, 712. https://doi.org/10.3389/fmars.2019.00712

Gawarkiewicz, G., & Mercer, A. M. (2019). Partnering with fishing fleets to monitor ocean conditions. *Annual Review of Marine Science*, *11*, 391–411. https://doi.org/10.1146/annurev-marine-010318-095201

Gawarkiewicz, G., & Plueddemann, A. J. (2020). Scientific rationale and conceptual design of a process-oriented Shelfbreak observatory: The OOI Pioneer Array. *Journal of Operational Oceanography*, *13*, 19–36. https://doi.org/10.1080/1755876x.2019.1679609

Gawarkiewicz, G., Todd, R. E., Zhang, W. G., Partida, J., Gangopadhyay, A., Fratantoni, P., et al. (2018). The changing nature of shelfbreak exchange revealed by the OOI Pioneer Array. *Oceanography*, *31*, 60–70. https://doi.org/10.5670/oceanog.2018.110

Gawarkiewicz, G. G., Todd, R. E., Plueddemann, A. J., Andres, M., & Manning, J. P. (2012). Direct interaction between the Gulf Stream and the shelfbreak south of New England. *Scientific Reports*, *2*. https://doi.org/10.1038/srep00553

Glenn, S. M., & Ebbesmeyer, C. C. (1994). The structure and propagation of a Gulf Stream frontal eddy along the North Carolina Shelf Break. *Journal of Geophysical Research*, *99*, 5029–5046. https://doi.org/10.1029/93jc02786

Hersbach, H., Bell, B., Berrisford, P., Hirahara, S., Horányi, A., Muñoz-Sabater, J., et al. (2020). The ERA5 global reanalysis. *The Quarterly Journal of the Royal Meteorological Society*, *146*, 1999–2049. https://doi.org/10.1002/qj.3803

Holliday, N. P., Bersch, M., Berx, B., Chafik, L., Cunningham, S., Florindo-López, C., et al. (2020). Ocean circulation causes the largest freshening event for 120 years in eastern subpolar North Atlantic. *Nature Communications*, *11*, 585. https://doi.org/10.1038/s41467-020-14474-y

Hoskins, B. J. (1982). The mathematical theory of frontogenesis. *Annual Review of Fluid Mechanics*, *14*, 131–151. https://doi.org/10.1146/annurev.fl.14.010182.001023

Hoskins, B. J., & Bretherton, F. P. (1972). Atmospheric frontogenesis models: Mathematical formulation and solution. *Journal of the Atmospheric Sciences*, *29*, 11–37. https://doi.org/10.1175/1520-0469(1972)029<0011:afmmfa>2.0.co;2

Houghton, R. W., Aikman, F., & Ou, H. W. (1988). Shelf-slope frontal structure and cross-shelf exchange at the New England shelfbreak. *Continental Shelf Research*, *8*, 687–710. https://doi.org/10.1016/0278-4343(88)90072-6

Joyce, T. M. (1984). Velocity and hydrographic structure of a gulf stream warm-core ring. *Journal of Physical Oceanography*, *14*, 936–947. https://doi.org/10.1175/1520-0485(1984)014<0936:vahsoa>2.0.co;2

Joyce, T. M., Bishop, J. K. B., & Brown, O. B. (1992). Observations of offshore shelf-water transport induced by a warm-core ring. *Deep-Sea Research*, *39*, S97–S113. https://doi.org/10.1016/s0198-0149(11)80007-5

Joyce, T. M., Kwon, Y.-O., & Yu, L. (2009). On the relationship between synoptic wintertime atmospheric variability and path shifts in the Gulf Stream and the Kuroshio Extension. *Journal of Climate*, *22*, 3177–3192.

Kennelly, M. A., Evans, R. H., & Joyce, T. M. (1985). Small-scale cyclones on the periphery of a Gulf Stream warm-core ring. *Journal of Geophysical Research*, *90*, 8845–8857. https://doi.org/10.1029/jc090ic05p08845

Lee, C. M., & Brink, K. H. (2010). Observations of storm-induced mixing and Gulf Stream Ring incursion over the southern flank of Georges Bank: Winter and summer 1997. *Journal of Geophysical Research*, *115*. https://doi.org/10.1029/2009JC005706

Lee, T. N., Atkinson, L. P., & Legeckis, R. (1981). Observations of a Gulf Stream frontal eddy on the Georgia continental shelf, April 1977. *Deep-Sea Research Part A. Oceanographic Research Papers*, *28*, 347–378. https://doi.org/10.1016/0198-0149(81)90004-2

Lentz, S., Shearman, K., Anderson, S., Plueddemann, A., & Edson, J. (2003). Evolution of stratification over the New England shelf during the Coastal Mixing and Optics study, August 1996–June 1997. *Journal of Geophysical Research*, *108*, 3008. https://doi.org/10.1029/2001jc001121

Lentz, S. J. (2008a). Observations and a model of the mean circulation over the Middle Atlantic bight continental shelf. *Journal of Physical Oceanography*, *38*, 1203–1221. https://doi.org/10.1175/2007jpo3768.1

Lentz, S. J. (2008b). Seasonal variations in the circulation over the Middle Atlantic bight continental shelf. *Journal of Physical Oceanography*, *38*, 1486–1500. https://doi.org/10.1175/2007jpo3767.1

Lentz, S. J. (2010). The mean along-isobath heat and salt balances over the Middle Atlantic bight continental shelf. *Journal of Physical Oceanography*, *40*, 934–948. https://doi.org/10.1175/2009jpo4214.1

Lentz, S. J., Butman, B., & Harris, C. (2014). The vertical structure of the circulation and dynamics in Hudson Shelf Valley. *Journal of Geophysical Research: Oceans*, *119*, 3694–3713. https://doi.org/10.1002/2014jc009883

Lin, X., & Yang, J. (2011). An asymmetric upwind flow, Yellow Sea Warm Current: 2. Arrested topographic waves in response to the northwesterly wind. *Journal of Geophysical Research*, *116*. https://doi.org/10.1029/2010jc006514

Linder, C. A., & Gawarkiewicz, G. G. (1998). A climatology of the shelfbreak front in the Middle Atlantic Bight. *Journal of Geophysical Research*, *103*(18), 405423–406418. https://doi.org/10.1029/98jc01438

Lucey, S. M., & Nye, J. A. (2010). Shifting species assemblages in the Northeast US Continental Shelf large marine ecosystem. *Marine Ecology Progress Series*, *415*, 23–33. https://doi.org/10.3354/meps08743

Luther, M. E., & Bane, J. M. (1985). Mixed instabilities in the Gulf Stream over the continental slope. *Journal of Physical Oceanography*, *15*, 3–23. https://doi.org/10.1175/1520-0485(1985)015<0003:miitgs>2.0.co;2

Mason, E., Molemaker, J., Shchepetkin, A. F., Colas, F., McWilliams, J. C., & Sangrà, P. (2010). Procedures for offline grid nesting in regional ocean models. *Ocean Modelling*, *35*, 1–15. https://doi.org/10.1016/j.ocemod.2010.05.007

McWilliams, J. C. (2021). Oceanic frontogenesis. *Annual Review of Marine Science*, *13*, 227–253. https://doi.org/10.1146/annurev-marine-032320-120725

Mills, K., Pershing, A., Brown, C., Chen, Y., Chiang, F.-S., Holland, D., et al. (2013). Fisheries management in a changing climate: Lessons from the 2012 ocean heat wave in the Northwest Atlantic. *Oceanography*, *26*, 191–195. https://doi.org/10.5670/oceanog.2013.27

Morgan, C. W., & Bishop, J. M. (1977). An example of Gulf Stream eddy-induced water exchange in the Mid-Atlantic bight. *Journal of Physical Oceanography*, *7*, 472–479. https://doi.org/10.1175/1520-0485(1977)007<0472:aeogse>2.0.co;2

Nye, J. A., Link, J. S., Hare, J. A., & Overholtz, W. J. (2009). Changing spatial distribution of fish stocks in relation to climate and population size on the Northeast United States continental shelf. *Marine Ecology Progress Series*, *393*, 111–129. https://doi.org/10.3354/meps08220

Orlanski, I. (1976). A simple boundary condition for unbounded hyperbolic flows. *Journal of Computational Physics*, *21*, 251–269. https://doi.org/10.1016/0021-9991(76)90023-1

Pershing, A. J., Alexander, M. A., Hernandez, C. M., Kerr, L. A., Le Bris, A., Mills, K. E., et al. (2015). Slow adaptation in the face of rapid warming leads to collapse of the Gulf of Maine cod fishery. *Science*, *350*, 809–812. https://doi.org/10.1126/science.aac9819

Pershing, A. J., Mills, K. E., Dayton, A. M., Franklin, B. S., & Kennedy, B. T. (2018). Evidence for adaptation from the 2016 marine heatwave in the Northwest Atlantic Ocean. *Oceanography*, *31*, 152–161. https://doi.org/10.5670/oceanog.2018.213

Piecuch, C. G., Huybers, P., Hay, C. C., Kemp, A. C., Little, C. M., Mitrovica, J. X., et al. (2018). Origin of spatial variation in US East Coast sea-level trends during 1900–2017. *Nature*, *564*, 400–404. https://doi.org/10.1038/s41586-018-0787-6

Rypina, I. I., Chen, K., Hernández, C. M., Pratt, L. J., & Llopiz, J. K. (2019). Investigating the suitability of the Slope Sea for Atlantic bluefin tuna spawning using a high-resolution ocean circulation model. *ICES Journal of Marine Science*, *76*, 1666–1677. https://doi.org/10.1093/icesjms/fsz079

Sallenger, A. H., Doran, K. S., & Howd, P. A. (2012). Hotspot of accelerated sea-level rise on the Atlantic coast of North America. *Nature Climate Change*, *2*, 884–888. https://doi.org/10.1038/nclimate1597

Schlegel, R. W., Oliver, E. C. J., & Chen, K. (2021). Drivers of marine heatwaves in the Northwest Atlantic: The role of air–sea interaction during onset and decline. *Frontiers in Marine Science*, *8*. https://doi.org/10.3389/fmars.2021.627970

Scott, J. T., & Csanady, G. T. (1976). Nearshore currents off Long Island. *Journal of Geophysical Research*, *81*, 5401–5409. https://doi.org/10.1029/jc081i030p05401

Seidov, D., Baranova, O. K., Boyer, T., Cross, S. L., Mishonov, A. V., & Parsons, A. R. (2016). *Northwest Atlantic Regional Ocean Climatology*. NOAA Atlas NESDIS 80.

Spall, M. A. (1995). Frontogenesis, subduction, and cross-front exchange at upper ocean fronts. *Journal of Geophysical Research*, *100*, 2543–2557. https://doi.org/10.1029/94jc02860

Stommel, H., & Leetmaa, A. (1972). Circulation on the continental Shelf. *Proceedings of the National Academy of Sciences*, *69*, 3380–3384. https://doi.org/10.1073/pnas.69.11.3380

Todd, R. E., Gawarkiewicz, G. G., & Owens, W. B. (2012). Horizontal scales of variability over the middle Atlantic Bight Shelf break and continental rise from finescale observations. *Journal of Physical Oceanography*, *43*, 222–230.

Todd, R. E., Rudnick, D. L., Sherman, J. T., Owens, W. B., & George, L. (2017). Absolute velocity estimates from autonomous underwater gliders equipped with Doppler current profilers. *Journal of Atmospheric and Oceanic Technology*, *34*, 309–333. https://doi.org/10.1175/jtech-d-16-0156.1

Ullman, D. S., Codiga, D. L., Pfeiffer-Herbert, A., & Kincaid, C. R. (2014). An anomalous near-bottom cross-shelf intrusion of slope water on the southern New England continental shelf. *Journal of Geophysical Research: Oceans*, *119*, 1739–1753. https://doi.org/10.1002/2013jc009259

Warner, J. C., Sherwood, C. R., Arango, H. G., & Signell, R. P. (2005). Performance of four turbulence closure models implemented using a generic length scale method. *Ocean Modelling*, *8*, 81–113. https://doi.org/10.1016/j.ocemod.2003.12.003

Xu, F. H., & Oey, L. Y. (2011). The origin of along-shelf pressure gradient in the Middle Atlantic Bight. *Journal of Physical Oceanography*, *41*, 1720–1740. https://doi.org/10.1175/2011jpo4589.1

Yang, J., & Chen, K. (2021). The role of wind stress in driving the along-shelf flow in the Northwest Atlantic Ocean. *Journal of Geophysical Research: Oceans*, *126*, e2020JC016757. https://doi.org/10.1029/2020jc016757

Zhang, W. G., & Gawarkiewicz, G. G. (2015). Dynamics of the direct intrusion of Gulf Stream ring water onto the Mid-Atlantic Bight shelf. *Geophysical Research Letters*, *42*, 7687–7695. https://doi.org/10.1002/2015gl065530

Zhang, W. G., Gawarkiewicz, G. G., McGillicuddy, D. J., & Wilkin, J. L. (2011). Climatological mean circulation at the New England Shelf Break. *Journal of Physical Oceanography*, *41*, 1874–1893. https://doi.org/10.1175/2011jpo4604.1